

Received March 17, 2022, accepted May 1, 2022, date of publication May 10, 2022, date of current version May 18, 2022.

Digital Object Identifier 10.1109/ACCESS.2022.3174067

# Equivalent Electrical Circuits and Their Use Across Electrochemical Impedance Spectroscopy Application Domains

MAXIME VAN HAEVERBEKE<sup>ID</sup>, MICHEL STOCK<sup>ID</sup>, AND BERNARD DE BAETS<sup>ID</sup>

KERMIT Research Unit, Department of Data Analysis and Mathematical Modelling, Ghent University, 9000 Ghent, Belgium

Corresponding author: Maxime Van Haeverbeke (maxime.vanhaeverbeke@ugent.be)

This work was supported by the Research Foundation—Flanders (FWO) under Grant FWO-SBO S007019N (Bisceps).

**ABSTRACT** When studying electrochemical systems, EIS practitioners face the challenge of choosing a relevant equivalent electrical circuit to analyze their measurement data and interpreting the role of its components. In this review, we take a closer look at the use of equivalent electrical circuits (EEC) across various application domains. We aim to aid EIS practitioners in determining and evaluating their EEC-based data analysis methodology in light of recent progress from all EIS application domains. We review EEC usage and its interpretation while additionally providing software to automatically search for equivalent electrical circuits from the relevant application domain literature that fit EIS measurements supplied by users. Finally, we make a comparison of the impedimetric behaviour and circuit modelling approaches of a range of different electrochemical systems and discuss some complementary EIS data analysis strategies.

**INDEX TERMS** Electrochemical impedance spectroscopy, equivalent electrical circuit, battery, supercapacitor, fuel cell, corrosion, cement, plant, biosensor.

## I. INTRODUCTION

### A. ELECTROCHEMICAL IMPEDANCE SPECTROSCOPY

Electrochemical impedance spectroscopy (EIS) is a widely used technique to examine the properties of electrochemical systems. It provides an indirect means to measure a variety of electrochemical quantities that are otherwise hard to assess accurately. Such quantities include the corrosion rate of metals [1], the state of charge of batteries [2], the physiological state of plants [3], and many more. A generalized version of Ohm's law describes the impedance  $Z(\omega)$  of a given system at radial frequency  $\omega$ :



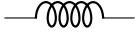

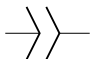
$$Z(\omega) = \frac{\mathcal{F}\{V(t)\}}{\mathcal{F}\{I(t)\}} = \frac{\tilde{V}(\omega)}{\tilde{I}(\omega)}, \quad (1)$$

where  $\mathcal{F}$ ,  $V(t)$ ,  $I(t)$ ,  $\tilde{V}(\omega)$  and  $\tilde{I}(\omega)$  denote the Fourier transformation, time domain voltage over the system, time domain current, frequency domain voltage and frequency domain current, respectively. In EIS, the impedance that a given sample presents when subjected to a small sinusoidal input voltage or current perturbation is evaluated over a range of frequencies. The resulting set of impedance values form the

The associate editor coordinating the review of this manuscript and approving it for publication was Yasar Amin<sup>ID</sup>.

system's impedance spectrum under the prevailing environmental conditions (e.g., temperature and applied voltage) at the time of measurement [4]–[6]. While the determination of the resistance of an electrolyte by means of alternating current measurements dates back about 150 years, the development of commercial frequency response analyzers and the accompanying software at the end of the last century instigated a rapid proliferation of the use of EIS in a variety of application domains [7]. EIS is a non-invasive and very information-dense method, allowing practitioners to disentangle the various electrochemical processes taking place within the system. Furthermore, it is relatively fast and easy to implement with the modern commercial instrumentation that is currently available. It partially owes its popularity to its amenability to automation and online measurement and its label-free nature [8] in biosensing applications. With the advent of modern microelectronics, a transition from initially being limited to lab environment system characterization to real-time measurements in the field is making rapid progress. Some disadvantages of EIS include the requirement of expensive equipment and its theoretical complexity, which makes it not as easy to interpret as some alternative methods. This review primarily covers the aspects of EIS related to equivalent electrical circuits. Aside from providing an overview

TABLE 1. Common equivalent circuit components.

Component	Name	Z Equation
	Resistor	(2)
	Capacitor	(4)
	Inductor	(5)
	Warburg	(7)
	CPE	(6)

of equivalent electrical circuits (EECs) and their contemporary developments, our contributions include new ways to compare circuit topologies and impedance spectra, software to find matching circuits per application, and insights into the similarity of different electrochemical systems and the limited section of the circuit topology space taken up by practically applied EECs. We limit our scope to equivalent electrical circuits and their use when analysing EIS measurements. A recent general review of EIS was made by Wang et al. [9]. Considerations concerning the experimental setup of EIS, including the choice of appropriate probe configurations and hardware, can also be found elsewhere [5].

**B. EQUIVALENT CIRCUITS AND THEIR COMPONENTS**

Equivalent electrical circuits are the standard tool for analyzing EIS measurements. When applied correctly, they can provide an approximate mechanistic interpretation of the considered electrochemical system. The electrical elements present in the circuits can be split into two categories (the naming conventions of which differs between applications): *integer-order elements* and *fractional-order elements*. The integer-order elements typically found in equivalent circuits are resistors, capacitors, and inductors, whereas the regularly applied fractional elements are the constant phase element (CPE) and the Warburg element (the latter being a special case of the former). Table 1 displays these five common circuit components. The impedance over the integer-order components can be calculated by applying the Fourier transformation to the expressions of the voltage over them in the time domain, and rearranging. The voltage over a resistor in the time domain is given by  $V(t) = RI(t)$ . Taking the Fourier transformation of the time-dependent variables and rearranging, we get

$$R = \frac{\tilde{V}(\omega)}{\tilde{I}(\omega)} = Z_R(\omega). \tag{2}$$

From Eq. (2), we see that the impedance over a resistor is frequency independent and equal to its resistance value. When a resistor is connected in series in a circuit, one notices a shift on the real axis of the spectrum in the Nyquist plot, which displays the imaginary part of the impedance as a

function of the real part. The voltage over a capacitor in the time domain is given by  $V(t) = \frac{1}{C} \int I(t) dt$ , where  $C$  is the capacitance measured in Farad. Taking the Fourier transformation of the time-dependent variables and bearing in mind that the Fourier transform of the integral of a function is equal to the Fourier transform of the function divided by  $\omega j$ , where  $j$  is the imaginary unit, we get

$$\tilde{V}(\omega) = \frac{1}{C} \frac{\tilde{I}(\omega)}{\omega j}, \tag{3}$$

so that the impedance of a capacitor can be calculated as

$$Z_C(\omega) = \frac{1}{C \omega j}. \tag{4}$$

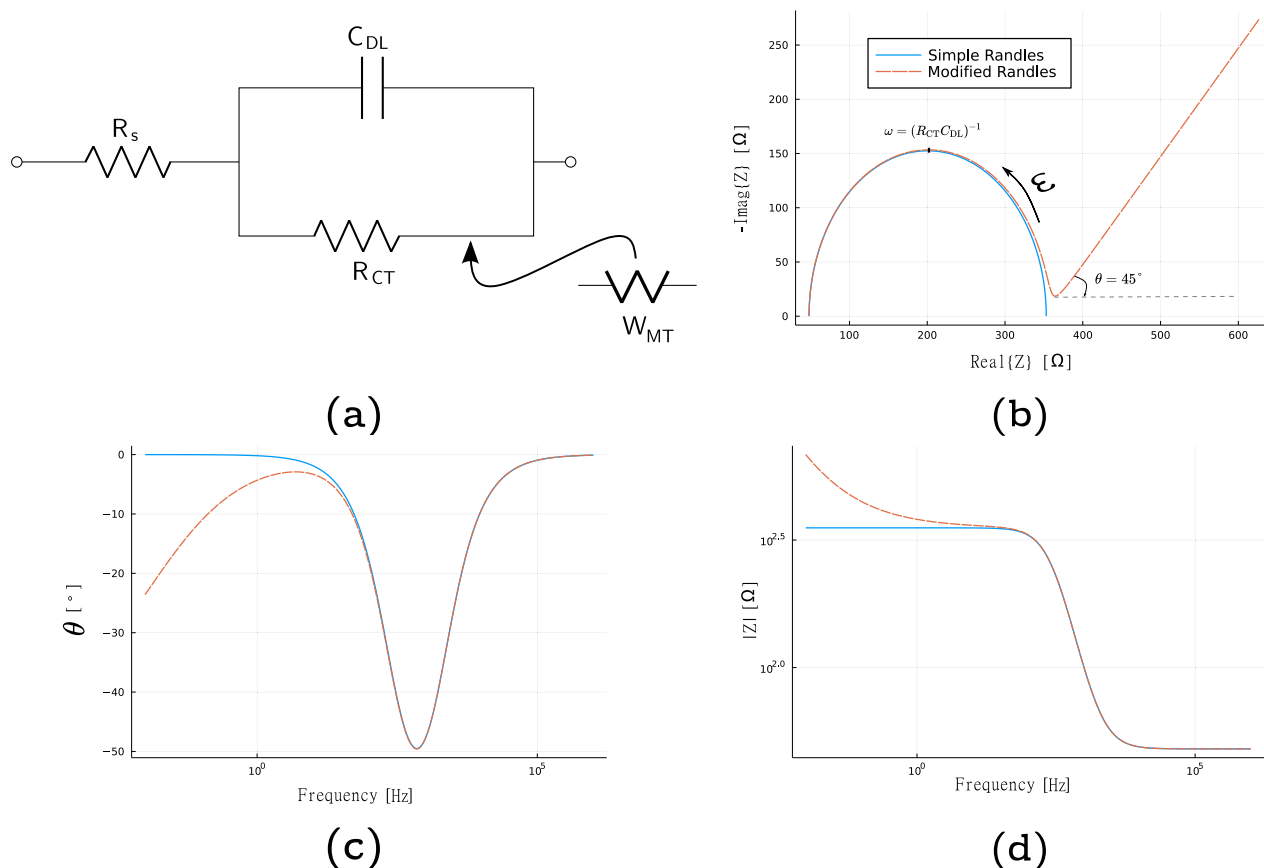
The voltage over an inductor in the time domain is given by  $V(t) = L \frac{dI(t)}{dt}$ , where  $L$  is the inductance measured in Henry. Taking the Fourier transformation of the time-dependent variables with the knowledge that the Fourier transform of the derivative of a function is equal to the Fourier transform of that function multiplied by  $\omega j$ , we get

$$Z_L(\omega) = L \omega j. \tag{5}$$

Inductors are often present in battery impedance models, where they are used to model inductive effects caused by cell windings and the cables connecting the battery to the potentiostat during measurement. Bode plots display the magnitude and phase angle of a complex-valued impedance spectrum as a function of the perturbation frequency. When examining the impedimetric behavior of a system using Bode plots, it is useful to note that resistors do not cause a phase shift between the voltage and the current, capacitors cause a  $-90$  degrees phase shift, and inductors cause a  $+90$  degrees phase shift. Idealized (integer-order) components do not describe reality exactly, but merely describe reality *conveniently*, as they have a straightforward electrical interpretation. The total impedance transfer function over a system represented by an equivalent circuit can be calculated through the application of Kirchoff’s laws, in combination with the individual components’ impedance expressions. The total impedance of serially connected components equals the sum of their impedances, whereas the impedance of parallelly connected components is the inverse of the sum of their inverted impedances. Note that the order of the components in an EEC does not influence its impedance spectrum, so that a given circuit can be displayed in different ways. In general, the configuration that lends itself to the clearest physical interpretation should be selected. A difficulty of only using integer-order components is that they are only capable of modelling systems that display ideal behavior. In real systems, the introduction of fractional circuit components is often necessary. The impedance of a CPE is given by

$$Z_{CPE}(\omega) = \frac{1}{Y_0(j\omega)^\alpha}, \tag{6}$$

where  $Y_0$  is the CPE constant and  $\alpha$  is the CPE exponent. CPE exponent values of  $-1, 0, 1/2$  and  $1$  allow for the CPE component to represent an inductor, resistor, Warburg element,



**FIGURE 1.** (a) Simple Randles circuit with its modification to account for Warburg diffusion. (b) Nyquist plots of the simple Randles circuit and its modification. The direction of increasing frequencies is indicated, as is the time constant's corresponding critical frequency. The parameters used for this simulation are  $R_s = 48\Omega$ ,  $C_{DL} = 2 \times 10^{-6}F$ ,  $R_{CT} = 304\Omega$ , and  $\sigma = 71\Omega s^{-1/2}$ . (c) Phase angle Bode plot of the simple Randles circuit and its modification. (d) Impedance magnitude Bode plot of the simple Randles circuit and its modification.

and a capacitor, respectively. In real systems, capacitors are typically replaced by CPEs. Such replacement also improves the fit of the other circuit parameters, allowing for a more accurate analysis. For instance, the double-layer effect (i.e., the accumulation of two layers of polarized ions near the electrode surface after the application of an electric potential) [10] is theoretically modelled by a capacitor, yet in many practical applications the electrode double-layer capacitance is not consistent with a pure capacitance due to electrode surface roughness and other non-uniformities. For this reason, the use of a CPE instead has become common practice. The Warburg element is often used to model mass-transfer processes (diffusion processes) and gives rise to a 45-degree slope in the Nyquist plot (see Fig. 1). The impedance over such a Warburg element is given by

$$Z_W(\omega) = \sigma \omega^{-1/2} - j\sigma \omega^{-1/2}, \tag{7}$$

where  $\sigma$  is the Warburg coefficient (measured in  $\Omega s^{-1/2}$ ), related to the diffusion coefficient and the bulk concentration of charged species. Many works model a Warburg element as a CPE with  $\alpha = 1/2$ . In this case the Warburg coefficient can be retrieved from the  $Y_0$  parameter of the CPE with  $\sigma = \frac{1}{\sqrt{2}Y_0}$ .

It has been concluded in several works that fractional-order circuit models typically yield a better and more noise-robust fit to experimental data without having to make the circuit topology overly involved, at the cost of a somewhat less straightforward interpretation [11]. The replacement of a capacitor by a CPE only adds one additional parameter, while potentially greatly improving the fit. Only using ideal circuit elements yields perfect semi-circles in the Nyquist plot, which can at best only roughly approximate real data. Another argument in favor of fractional-order circuit models is that integer-order models cannot distinguish between small changes in the EIS results, making them unsuitable to model the subtle changes in Faradaic impedance seen in some electrochemical phenomena. For instance, the use of CPEs aids the simulation of realistic reaction conditions with porous electrodes, yielding an improved fit over a wide frequency range. CPEs have also been interpreted as the combination of a resistor and a capacitor by modelling a trade-off between capacitance and resistance as  $\alpha$  varies. CPE behavior can be recreated with a long series of resistors and capacitors, also referred to as a transmission-line circuit. Transmission-line circuits are an alternative EIS circuit modelling approach that theoretically models the electrode-electrolyte interface of porous electrodes [12].

Electrochemical systems can give rise to impedance spectra forming one or more semi-circles in a Nyquist plot. Resistors that are parallelly connected with capacitors produce such semi-circles. The characteristic frequency of such (sub-)circuits is the frequency at which the semi-circles in the Nyquist plot reach their apex. The inverse of this frequency is called the time constant  $\tau$ , calculated as  $\tau = (RC)^{-1}$ . Different electrochemical phenomena will typically each have their own characteristic time constant, which can be distinguished in the Nyquist plot, given that they do not significantly overlap. The parallel connection of a resistor and a CPE is commonly used in EECs modelling real systems, and is referred to in the literature as a ZARC element. Time constants can also be calculated for such elements:  $\tau = (RY_0)^{-1/\alpha}$ .

The Randles circuit describes the impedance of an electrode-electrolyte interface. The main electrochemical processes at this interface are the electrochemical double layer represented by a capacitor  $C_{DL}$  or CPE, the resistance to charge transfer by rate-limiting chemical reactions  $R_{CT}$ , and the equivalent series resistance  $R_S$ , caused by the electrode and electrolyte. In settings where the diffusion of chemical species in the neighborhood of the electrode becomes rate-limiting, the Randles circuit is modified to include a Warburg mass transfer impedance  $W_{MT}$ . The Randles circuit and its modification are displayed in Fig. 1, along with their characteristic Nyquist and Bode plots. The impedance transfer functions of the Randles circuit  $Z_{SR}$  and its modification  $Z_{MR}$  are

$$Z_{SR}(\omega) = R_S + \frac{R_{CT}}{R_{CT}C_{DL}\omega j + 1} \quad (8)$$

$$Z_{MR}(\omega) = R_S + \frac{R_{CT} + \frac{\sqrt{2}\sigma}{\sqrt{\omega j}}}{(R_{CT} + \frac{\sqrt{2}\sigma}{\sqrt{\omega j}})C_{DL}\omega j + 1}. \quad (9)$$

Through examination of Eqs. (8) and (9) along with the circuit and plots in Fig. 1, the system can be interpreted. At high frequencies, the impedance over the capacitor and Warburg element is negligible. The current flows through the top parallel branch in the circuit, and the impedance is given by  $R_S$ . At intermediate frequencies, the capacitor contributes to the impedance, causing the phase angle to deflect towards  $-90$  degrees. At low frequencies, the impedance over the capacitor is high, causing all of the current to flow through the bottom parallel branch, yielding an impedance of  $R_{CT}+R_S$  for the simple Randles circuit. For the modified Randles circuit, the Warburg diffusion impedance dominates.

### C. EQUIVALENT CIRCUIT PARAMETER IDENTIFICATION

Several mathematical optimization methods have been proposed for the identification of equivalent circuit parameters on the basis of EIS measurement data. The parameter identification is either conducted once after obtaining the measurements, or it is done continuously to monitor dynamic systems in real-time, for example, in health state monitoring in battery management systems [13]. During EEC parameter optimization, it is advisable to restrict the parameter ranges

TABLE 2. Parameter identification methods.

Optimization method	References
Levenberg–Marquardt	[19]
Differential evolution	[20]
Genetic algorithms	[21]–[23]
Nelder–Mead simplex	[15], [24], [25]
Fractional-order techniques	[26], [27]
Particle filter	[28]
Particle swarm optimization	[14], [29], [30]

of the components to physically relevant regions, making use of domain knowledge if possible [14], [15]. The earliest parameter extraction strategy was a graphical one, where rough estimates of the parameter values can be obtained through examination of the Nyquist plots of relatively simple electrochemical systems. A non-exhaustive overview of contemporary EEC parameter optimization methods, along with examples of a few reference works in which they are applied, can be found in Table 2. Some of these methods require the users to input initial parameter guesses, making the quality of the fit dependent on the expertise of the users. The aforementioned graphical parameter estimation method and the distribution of relaxation times (DRT, see Section I-D) can be useful to find reasonable initial parameter values that are promptly provided to one of those optimization methods. Several recently developed parameter optimization methods make use of a two-step parameter identification, where a first optimization method provides the initial values of a second parameter optimization method for further fine-tuning of the parameter values. An effective two-step parameter identification strategy described in [16], [17] consists of a differential evolution step that does not require initial parameter guesses, followed by a Nelder–Mead simplex fine-tuning step. This parameter identification approach is also adopted in the software accompanying this work (see Section II). Apart from using a fitness threshold and doing a visual comparison of the impedance measurements and the impedance spectrum simulated using the fitted parameters, checking whether the residuals are more or less randomly distributed, without obvious systematic errors, is a way to evaluate whether a given combination of EEC and parameter values is acceptable [18].

Besides the optimization method used, also the chosen objective function is a vital aspect of the circuit parameter identification procedure to be considered. Using the mean squared error is inadvisable, as it disregards the frequency information, causing undesired implicit weighing effects [23]. For this work, the performance of a variety of objective functions from the literature (mainly differing in their weighing method) [15], [16], [23], [31]–[35] were compared on simulated data from several different equivalent circuits. This comparison was done by evaluating the fits on the basis of the parameter values resulting from the optimization of the tested objective functions. The objective function  $F(\Theta)$  that performed best overall is given by

$$F(\Theta) = \frac{1}{N} \sum_{n=1}^N \frac{|Z_{m,n} - Z_{t,n}(\Theta)|^2}{|Z_{m,n}|^2 + |Z_{t,n}(\Theta)|^2}. \quad (10)$$

Here,  $N$  denotes the number of measurements,  $Z_m$ ,  $n$  the measured impedance at the  $n$ th measured frequency and  $Z_t$ ,  $n(\Theta)$  the model estimate of the impedance at the  $n$ th measured frequency with parameters  $\Theta$ .

#### D. COMPLEMENTARY DISTRIBUTED PARAMETER METHODS

The EIS data representation toolbox has witnessed some new additions in recent years. The classic but effective Bode and Nyquist plot data representations along with equivalent circuit analysis have been augmented with promising complementary analysis methodologies, which at the same time improve the utility of equivalent circuit analysis. The model-free distribution of relaxation times (DRT) [36], [37] is an emerging distributed parameter method that sheds light on hard-to-interpret cases where the system-under-test contains electrochemical processes with similar time constants [38]. Frequency-domain impedance measurements are transformed to the time constant domain, where various relaxation processes can be examined. In addition, it can also aid in various aspects of equivalent circuit analysis such as EEC topology establishment or confirmation [39], providing reasonable initial values for the parameter optimization methods that require them, and EEC parameterisation [40]. The relation between the impedance spectrum in the frequency domain  $Z(\omega)$  and the DRT  $\gamma(\tau)$  in the time domain, for measurements fulfilling the validity criteria discussed in Section I-E, is given by:

$$Z(\omega) = R_0 + \int_0^{\infty} \frac{\gamma(\tau)}{1 + j\omega\tau} d\tau, \quad (11)$$

where  $R_0$  is the pure resistance of the system (i.e., the value of the real-valued impedance at the point where the spectrum crosses the horizontal axis in the Nyquist plot) and  $\tau$  is the relaxation time. To date, the DRT method has mainly come to fruition in power source applications. Other applications would likely also benefit from the inclusion of such an analysis within their research and development. Tikhonov regularization is currently the most successful method to obtain a DRT profile with unmeasured regions of the curve smoothed out. A drawback is the need to choose an appropriate value for the regularization parameter  $\lambda$ . This parameter determines the smoothness of the resulting DRT profile and needs to be chosen with great care, as too low values will cause artefacts in the DRT, whereas too high values will decrease the resolvability of the peaks. Both scenarios lead to false insights about the system. A requirement of the DRT method is high-quality impedance measurements with a high-frequency resolution, as measurement errors or noise can also cause incorrect DRT profiles. These relatively strict requirements may be a reason why the method's use is currently still limited to power source applications. Research is being conducted to mitigate the drawbacks of DRT [41]–[43]. Besides DRT, the emerging Distribution of Diffusion Times (DDT) [44] also holds promise as a complementary method to supplement the insights gained from EEC analysis [43].

#### E. NOISE IN EIS MEASUREMENTS AND DATA VALIDATION

The EIS measurements need to fulfill a few conditions to conduct a meaningful analysis of the electrochemical system under study. The three main requirements that EIS measurements should meet are termed linearity, stability, and causality. The **linearity** condition states that the system has to obey Ohm's law. The impedance magnitude should be independent of the magnitude of the input perturbation signal. The applied sinusoidal perturbation and impedance response must be at the same frequency, with no additional frequencies (harmonics) generated during the experiment. In reality, electrochemical systems are not linear. Pseudo-linearity is attained by using an appropriately small perturbation amplitude (e.g., 10mA). Excessively large excitation amplitudes give rise to noise caused by harmonics in the impedance response. The choice of the input signal amplitude signifies a trade-off between signal-to-noise ratio issues at too small amplitudes and non-linearity problems at too large amplitudes. **Stability** refers to the requirement that the system remains unchanged within the experiment's time frame. Its state before and after the input perturbation should remain the same, without drift. To maintain the stability of the system while analyzing complex systems, the experiment time frame should be kept in check by not using too low frequencies for which the response takes longer to evaluate. This issue is also addressed with the application of the multi-sine method, in which multiple frequencies are measured at the same time [45]. When applicable, stability can be checked by comparing the open-circuit potential before and after the experiment. Finally, the **causality** condition requires that the impedance response only arises due to the input perturbation, and is not due to instrument artefacts or other processes. Appropriate measures to avoid noise in the system are application dependent. Practitioners should take precautionary measures to avoid noise before the experiments and evaluate the validity of their data afterwards. Some precautionary measures include using a reliable reference electrode, the use of a Faraday cage to avoid noise caused by interference in some applications, ensuring the absence of short leads, checking for wire issues (rusty wires will influence the impedance), use of shielded wires, and so on. Several methodologies have been developed to check the validity of the measurements. The Kramers–Kronig (KK) relations are a useful way to check data validity [46]. They are given by:

$$Z'(\omega) = Z'(\infty) + \frac{2}{\pi} \int_0^{\infty} \frac{xZ''(x) - \omega Z''(\omega)}{x^2 - \omega^2} dx \quad (12)$$

and

$$Z''(\omega) = -\frac{2\omega}{\pi} \int_0^{\infty} \frac{Z'(x) - Z'(\omega)}{x^2 - \omega^2} dx. \quad (13)$$

They state that the real and imaginary parts (or alternatively the phase and magnitude) of a system's impedance spectrum are related. The impedance magnitude is calculated from the phase, after which it is compared to the experimental data. If there is no match, at least one of the three requirements

is not met. Use of the KK relations can identify invalid data, but does not completely guarantee data validity. Some artifacts will comply with the KK relations, due to them also being valid circuit elements (e.g., the cable capacitance of the potentiostat can contribute to the impedance of systems with very small capacitance values). Another classical check is the examination of accuracy contour plots prior to measurement, which is required to avoid measurement errors caused by the wires connecting the instrument to the cell. An often used linear variant of the KK transform was developed by Boukamp [47], and further refined by Schönleber *et al.* [48]. Further research on EIS measurement validation strategies is ongoing. Some useful recent developments include Total Harmonic Distortion (THD) to evaluate the linearity of the system response [49], and drift correction to mitigate the instability of the system, at the cost of quantitative interpretability (qualitative interpretation remains). The measurement error structure theory developed by Orazem *et al.* [50] provides a means to model the different kinds of measurement errors encountered during EIS experiments.

## F. COMPARING CIRCUIT TOPOLOGIES AND IMPEDANCE SPECTRA

Here, we outline some of the mathematical tools that will be used to compare circuits and their spectra.

### 1) MULTISSET JACCARD INDEX

The Jaccard or Tanimoto index [51] is a measure for the similarity of sample sets. It is defined as the ratio of the cardinalities of the intersection and the union of the sets

$$J(A, B) = \frac{|A \cap B|}{|A \cup B|} = \frac{|A \cap B|}{|A| + |B| - |A \cap B|}. \quad (14)$$

Multisets are extensions of sets, allowing for the presence of multiple instances of their elements. A few relevant definitions and properties of multisets are listed below [52].

- (i) The multiplicity  $m_A(x)$  of an element  $x$  of a multiset  $A$  is the number of times it occurs within that multiset.
- (ii) The Support  $\text{Supp}$  of a multiset is its corresponding set (with one instance per element).
- (iii) The cardinality of a multiset is the sum of the multiplicities of each of its elements:

$$|A| = \sum_{x \in \text{Supp}(A)} m_A(x).$$

- (iv) The union of two multisets  $A$  and  $B$  is the multiset  $C$ , where the multiplicity of each of its elements is given by the maximum multiplicity of that element in  $A$  and  $B$ :  $m_C(x) = \max(m_A(x), m_B(x))$ .
- (v) The intersection of two multisets  $A$  and  $B$  is the multiset  $C$ , where the multiplicity of each of its elements is given by the minimum multiplicity of that element in  $A$  and  $B$ :  $m_C(x) = \min(m_A(x), m_B(x))$ .

Bearing the above definitions in mind, the Jaccard index for two multisets  $A$  and  $B$ , taking values in  $[0, 1]$ , is given by

$$J(A, B) = \frac{\sum_{x \in C} \min(m_A(x), m_B(x))}{\sum_{x \in C} \max(m_A(x), m_B(x))}, \quad (15)$$

where  $C = \text{Supp}(A) \cup \text{Supp}(B)$ . In this work, the multiset Jaccard index is used as a similarity measure between circuit topologies, where each circuit is represented by the multiset of circuit elements and parallel or serial connections of which it is composed (e.g., a series or parallel system of three components counts for two corresponding connections). In this way, the simple Randles circuit in Fig. 1a, is composed of two resistors, a capacitor, a series operation and a parallel operation.

### 2) DISTANCE MEASURE FOR EIS SPECTRA

In order to assess the similarity between equivalent electrical circuits of different electrochemical systems, it is interesting to not only consider their topology, but also the values of their parameters. The information contained in the combination of a circuit topology and the values of its parameters is equivalent to the information contained in its noiseless EIS spectrum over the appropriate range of frequencies. While there is a difference in the size of the numerical impedance measurements between the different applications, the shape of the spectra is more relevant than their order of magnitude when comparing impedance spectra from a mechanistic perspective. The cosine similarity measure is a suitable option in this context, as it compares vectors in a relative rather than an absolute way. Applications of this similarity measure are present in natural language processing [53], as well as the analysis of data originating from other spectroscopic techniques [54]–[56].

It is calculated as

$$S_{\cos}(A, B) = \frac{A \cdot B}{\|A\| \|B\|} = \frac{\sum_{i=1}^n A_i B_i}{\sqrt{\sum_{i=1}^n A_i^2} \sqrt{\sum_{i=1}^n B_i^2}}, \quad (16)$$

where  $A$  and  $B$  are the compared impedance spectra with their respective  $i$ -th component values  $A_i$  and  $B_i$ . For complex vectors, the magnitude of the cosine similarity value can be taken to obtain a real result. The cosine distance  $D_{\cos}(A, B)$  is defined as the complement of the cosine similarity:

$$D_{\cos}(A, B) = 1 - S_{\cos}(A, B). \quad (17)$$

## II. CHOOSING AN EQUIVALENT CIRCUIT

The choice of a reasonable EEC that lends itself to representing the studied electrochemical system adequately for a given purpose, is an important step of an EIS study. It should be noted that there are many cases where more than one EEC is capable of fitting a given set of EIS data [57], [58]. In these cases, there should be a preference for physically interpretable and less elaborate circuits. There are three potential strategies for choosing an EEC. The first strategy is an expert analysis, analyzing the various visual representations of the

measurements (particularly the Nyquist, Bode, and magnitude plots), in combination with sufficient prior knowledge of the system under study. Experts suggest plausible circuit configurations using knowledge of the involved physicochemical processes, after which they compare the models with experimental data and attempt to simplify the representation as much as possible. Experienced EIS users develop an intuition for the components that are likely to be present in a reasonable circuit topology, based on the Nyquist plots. In this way, a ZARC element gives rise to a depressed semi-circle in the Nyquist plot, whereas a serially-connected CPE typically causes an upward bend of the spectrum at low frequencies. Recent work features the application of DRT to support the equivalent electrical circuit topology decision [59].

The second and most often used strategy is to search through the literature for EIS analyses of similar systems. Some EIS systems are very commonly studied (e.g., Li-ion batteries). In cases where the electrochemical system under study already has a well-established EEC, it (or an appropriate variant taking study-specific differences into account) can conveniently be directly applied for further EIS analysis. Our software can expedite this step and is described in Section IV. This `circuit_search` functionality has been added to the previously developed `EquivalentCircuits.jl` package.

The third strategy is to make use of an equivalent circuit identification algorithm. When dealing with unknown electrochemical systems, the decision of which kind of circuit to use can be supported by appropriate software. In this way, researchers can conveniently see which kind of circuit topologies fit well to a given set of electrochemical impedance measurements. Such algorithms should be used with caution, as the physical justification of the circuits should not be neglected. The `circuit_evolution` functionality of the `EquivalentCircuits.jl` package suggests plausible circuit topologies capable of fitting a given set of impedance measurements [15]. Issues related to the interpretability and non-uniqueness of such algorithmically identified circuits are addressed by incorporating domain knowledge in the form of established circuit topologies from the literature, as well as taking measures to ensure that the simplest fitting circuit topology is identified. Regardless of how the circuit is obtained, one should devote enough attention to ensuring the physical relevance of the examined system before application.

### III. EQUIVALENT CIRCUITS IN DIFFERENT APPLICATION DOMAINS

The application domains of EIS contribute to the resolution of several of the largest contemporary global challenges, such as the transition to renewable energy, rapid prognosis and diagnosis of diseases, advances in monitoring and quality control in agriculture and food production, among others. The effective use of equivalent electrical circuits holds great promise in real-time applications and other in-situ applications where there are computational constraints or large amounts of data

to be analyzed. They can also be used as effective feature extractors, where EEC parameter acquisition is a preprocessing step in the data analysis pipeline. We discuss and consider circuit models of both integer and fractional order.

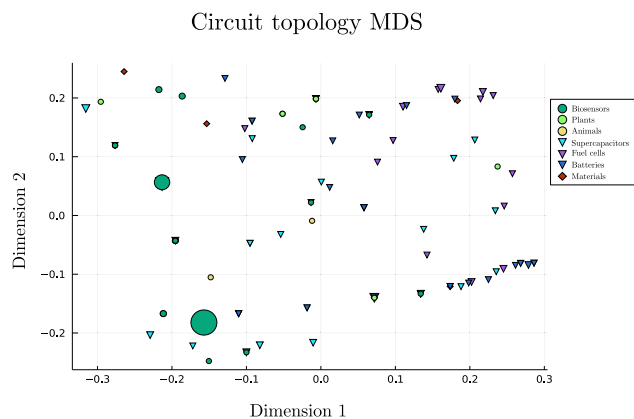
This review is structured around three large application categories: (i) power sources, (ii) materials science, and (iii) applications related to biology and food processing. Note that there are numerous applications at the interfaces between these categories. An example is the use of EIS for the analysis of microbial fuel cells [60]. Due to the versatility of EIS, there are inevitably many marginal applications, such as geological prospecting, archaeology, and soil moisture measurements, which are not covered here. The purpose of an EIS analysis across these application domains is usually the determination of in-situ and real-time diagnostics, the characterization of the existing electrochemical processes at the time of measurement, and the extraction of specific information about an analyzed process. The values of (a subset of) the equivalent circuit parameters can either directly or indirectly describe a process of interest. Typically, to indirectly obtain the value of a particular property of an electrochemical system, one fits the parameter values of an appropriate EEC and then uses a (typically linear) regression model with a selection or all of the EEC parameters as variables. A few circuits are applied widely for several different electrochemical systems and are mentioned here first. By far the most well-known circuits are the Randles circuit displayed in Fig. 1a and the single or double dispersion Cole models. The single dispersion Cole model is a simple Randles circuit with the substitution of the capacitor by a CPE element, while the double dispersion Cole model serially connects another ZARC element to the single dispersion Cole model. The latter was explicitly reviewed by Freeborn as being a fundamental fractional-order circuit with many applications [61]. These widely applied circuits are often favored because of their simplicity and acceptable fit to measurements. However, in many cases, their use lacks an adequate explanation of underlying physical mechanisms. While the biological application of EIS continues to proliferate, the vast majority of EIS usage still remains within non-biological contexts, such as corrosion analysis and non-destructive battery performance characterization. There are many opportunities in transferring progress and methodology from the most mature research areas to those lagging somewhat behind.

#### A. BIRDS-EYE VIEW OF EQUIVALENT CIRCUIT MODELLING

Equivalent electrical circuits were collected for each of the discussed domains of application. This was done through Web of Science queries using the keywords 'electrochemical impedance spectroscopy' AND 'equivalent circuit' appended by another AND operation with the application under consideration. We collected the equivalent circuit topologies and their fitted parameter values. When the parameter values were not directly available, we could obtain them with the two-step optimization strategy described in Section I-C after extrac-

tion of the impedance measurements from Bode plots using plot digitizing software and confirmation of the resulting reproduced Nyquist plot of the simulated impedance spectra, provided that these plots were reported. Circuit topologies are compared using the multiset Jaccard distance measure, which is the complement of Eq. (15). A multidimensional scaling (MDS) plot [62] of the collected circuit topologies, where the distance matrix was constructed using the aforementioned multiset Jaccard distance measure, is displayed in Fig. 2. The size of the observations in the plot is proportional to the number of times the circuit in question was encountered in the literature. It can be observed that several of the circuit topologies are concentrated in specific regions of the MDS plot. The largest observations of the biosensor circuits correspond to variations of the Randles circuit, which is predominantly used in this application. The cluster of battery circuits on the bottom left side corresponds to variations of the circuit topology displayed in Fig. 4. Furthermore, the left side of the plot is dominated by biological applications, whereas the right side is dominated by power sources, which typically use more complex circuit topologies. Supercapacitors appear to have the largest EEC diversity.

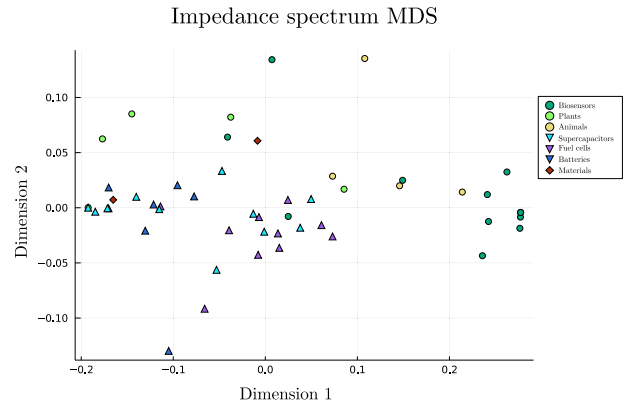
As the relevant frequency ranges differ between the different electrochemical systems, an intermediate frequency range of 10Hz to 10kHz was chosen to simulate impedance spectra. Only systems whose frequency range contains this interval were included. The resulting impedance spectra are compared in the MDS plot displayed in Fig. 3. The cosine distance from Eq. (17) is used for this comparison. An even clearer segregation of the different electrochemical systems can be seen here. The impedimetric behaviors of fuel cells and supercapacitors are rather similar.



**FIGURE 2.** 2D classical MDS visualisation of circuit topologies in different application domains, where the multiset Jaccard index from Eq. (15) was used. The size of the points corresponds to the relative number of collected circuits with this topology.

### B. POWER SOURCES

The application of EIS for the analysis of electrochemical power sources (batteries, fuel cells, and supercapacitors) is a hot topic due to the continued hype and development of electric vehicles and sustainable energy. The electrification of the



**FIGURE 3.** 2D classical MDS visualisation of impedance spectra in different application domains, where the cosine distance from Eq. (17) was used.

transport sector is one of the ways to alleviate humankind's current contribution to climate change. The unstable and intermittent delivery of renewable energy by wind turbines and solar panels is mitigated by further developing electrical energy storage systems. Two prominent roles of EIS in modern power sources are quality control and the provision of diagnostic system information to power source management systems. This diagnostic system information is derived from electrochemical reaction kinetics and interfacial characteristics that can be quantitatively analyzed using EIS. There is variety in the equivalent electrical circuits used in this application domain, as practitioners in this field will commonly expertly design equivalent electrical circuit models through inspection of the impedance spectrum's shape and time constants. The variety of components used is also more comprehensive, with the inductor element being significantly more common than in the circuits from, e.g., biological applications. The diagnostic information provided to power source management systems relates to the power sources' performance, life span, and safety. Parameters such as the State of Charge (SoC), the State of Health (SoH), and the State of Power (SoP) quantify this information. Testing the power sources under different operating conditions (e.g., current and temperature) provides information on the electrical dynamics of the device under test. Developing reliable prognostic and diagnostic algorithms is essential to assist energy management strategies. Some applications combine batteries, fuel cells, and supercapacitors to form hybrid energy sources, which can also be analyzed with EIS. A representative frequency range for EIS measurements on power sources is 10mHz to 100kHz, where the lower limit typically varies with an order of magnitude. For fuel cells, the upper limit is often in the order of 10kHz.

### 1) BATTERIES

Batteries are the most widely applied power sources present in most electronic devices. There are several chemical energy generation processes upon which modern batteries can rely, all of which EIS can analyze. These energy generation processes are based on redox reactions that can be categorized



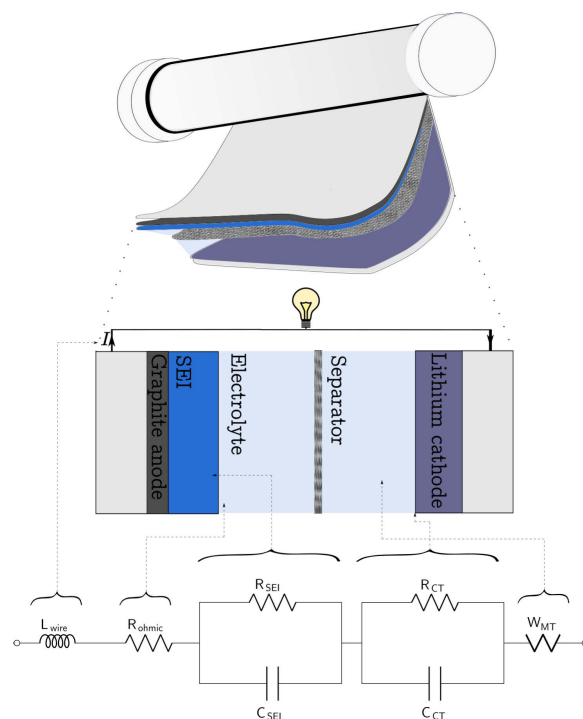
based on the various different chemical species used for energy generation [63]–[65], with the lithium-ion chemistry being the most successful in recent years [66], [67]. Monitoring the state of charge (SoC) and the state of health (SoH) [14], [68] of batteries are a few of the most developed applications of EIS. Battery SoH compares the current battery state to ideal (determining its aging degradation). Battery management systems (BMS) are required to optimize a battery's performance and ensure that it remains within safe operating limits, while maximizing the driving range. EIS informs them about safe and optimal energy usage and accurate battery state information, allowing for appropriate interventions when necessary. EIS hardware is complex and expensive, but research to feasibly include on-board EIS instrumentation in BMS is making progress [69], [70]. The battery-related applications of EIS are numerous, ranging from quality control/assurance to state estimation, monitoring of internal temperature, the influence of operating conditions, and degradation mechanisms.

The equivalent circuit-based interpretation of the typical Nyquist profile of batteries is generally composed of the ion-diffusion (and migration) effects at low frequencies, electrode reactions at middle frequencies, and inductive structure/wiring effects at high frequencies. The Warburg, RC (or ZARC), and inductor elements in Fig. 4 respectively model the above effects. Common variations include the addition or removal of serial ZARC elements [71], [72], The Warburg element placed in series with  $R_{CT}$  [73]–[75], omission of the inductor [76] or placement in parallel with a resistor [77], replacement of RC elements with a ZARC [74], [78], and combinations of the above. Transmission line circuits are also being applied to model the impedance spectra of batteries [71], [77].

## 2) FUEL CELLS

Fuel cells are energy generation elements that convert chemical energy into electricity through the oxidation of a fuel, typically hydrogen. Electricity is continuously produced when provided with a constant input flow of fuel and oxygen. Such cells can be categorized by their electrolyte, such as the proton-exchange membrane fuel cells (PEMFC) and the Solid Oxide fuel cells (SOFC), or by the fuel that is used instead of hydrogen (e.g., DMFC). A particular case is the microbial fuel cell (MFC), where the redox reactions that provide the current occur in bacterial cells [60]. Equivalent electrical circuit models have been applied in the modelling of fuel cell SoH, reaction kinetics, interfacial characteristics, and output power dynamics. Fuel cells are commonly integrated into a hybrid system consisting of a fuel cell stack (a combination of fuel cells in series or parallel), a battery, and a Balance of Plant (BoP), which roughly consists of the necessary tubing and air supply equipment. Some challenges relating to the cost, reliability, and durability of fuel cells need to be overcome to achieve their commercialization [79].

The electrolyte separating the anode and cathode is designed so that ions can pass through it, but not electrons,



**FIGURE 4.** Lithium-ion battery equivalent circuit model, where the capacitors modelling the solid electrolyte interface and electrochemical double layer are often replaced by CPEs when modelling real systems in practice.

effectively forcing the latter to pass through an external circuit (as a current) before arriving at the cathode. PEMFC membranes must remain hydrated at all times for efficient operation. EIS can be used to monitor a fuel cell's state of hydration, as well as to characterize several other relevant fuel cell properties [80], [81], using equivalent electrical circuits [82]. Fuel cells are energy efficient (use in co-generation can lead to more than 85% efficiency) and environmentally friendly, provided that the fuel is generated in a sustainable manner.

A fractional fuel cell EEC model is shown in Fig. 5. Some of the variations that occur in the literature include the parallel connection of an R-L sub-circuit to one of the electrodes [83], and a third serially connected ZARC element [84].

## 3) SUPERCAPACITORS

Supercapacitors are electrical energy storage devices characterized by fast charging and discharging cycles but lower energy density than batteries, meaning that the amount of energy stored relative to their volume or mass is lower. They were traditionally modelled using RC networks [85]. More recently, fractional-order circuit models containing a CPE or Warburg element are being applied in supercapacitor modelling [86]. Supercapacitors are categorized into three types according to their charge storage mechanism: (i) electrical double-layer capacitors (EDLC) that store energy electrostatically in Helmholtz electrical double layers [10], (ii) pseudocapacitors with electrochemical charge storage, where there is electron transfer between the electrodes and

electrolyte in fast redox reactions, and (iii) hybrid types where one electrode stores charge electrostatically, while the other stores charge electrochemically. The use of supercapacitors is advantageous in applications with a large charge demand in a short time frame. They are applied as voltage stabilizers (buffers) for power lines, which is of particular interest for renewable energy sources such as wind and photo-voltaic systems characterised by a fluctuating power supply. Supercapacitors are also emerging in the transport sector for rapid acceleration or for saving braking energy through power regeneration during deceleration. Another advantage of supercapacitors is that most of them do not rely on chemical reactions for their energy storage, which allows them to maintain their voltage capacity over long periods, as opposed to batteries that lose capacity more rapidly over time and use. The strengths of batteries and supercapacitors are combined in hybrid battery-supercapacitor systems in which the addition of a supercapacitor improves the longevity and performance of a battery. Supercapacitor EEC models are typically composed of two or three serially connected parts, the first of which is always a resistor. An example is given in Fig. 6. Some variations of this circuit include a Warburg diffusion element added in the Zarc element [87], [88], a ZARC element instead of the second CPE [89], [90], and the use of capacitors rather than CPEs in any of the above [91], [92]. Randles circuits are also frequently applied [93]–[95], as is the case with most applications. In supercapacitor applications an inductor is sometimes connected serially [96] in the Randles circuit.

C. MATERIALS SCIENCE

Materials science is a broad category, encompassing several subfields that make extensive use of EIS for the characterization of a given material’s property of interest. Some important EIS applications include construction material testing, corrosion monitoring and the characterization of polymer

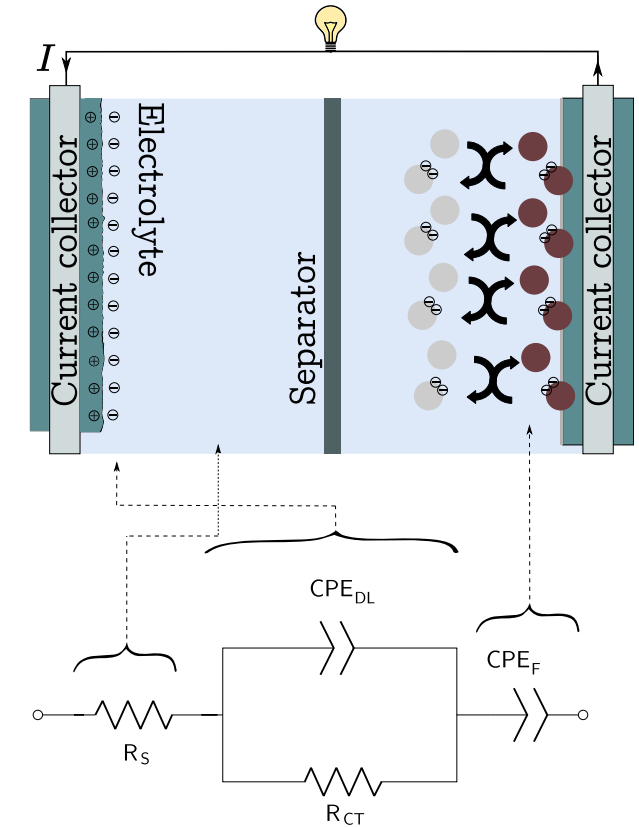


FIGURE 6. Exemplary hybrid supercapacitor circuit model.  $R_S$  models the electrolyte resistance,  $CPE_{DL}$  the non-ideal capacitance of the double layer,  $R_{CT}$  the charge transfer resistance and  $CPE_F$  the charge diffusion.

coatings (which are in turn used for corrosion inhibition). A link between this subsection and the previous one is that these materials are often electrochemically characterised and evaluated for their use in the fabrication of the discussed power sources. Besides the few large categories discussed here, EIS has also been applied for various miscellaneous material characterization studies, such as soils [97], polymers [98]–[100], alloys [101], and others.

1) COATINGS AND CORROSION MONITORING

Corrosion is an electrochemical redox process that can be microbially influenced (e.g., by sulfate-reducing bacteria) or solely be caused by a corrosive chemical environment, which is present in many industrial installations or electrochemical power sources. Determining corrosion rates of metals is essential to assess their suitability in specific industrial or biomedical settings and evaluate the effectiveness of corrosion protection measures. One of the most effective corrosion protection measures is the application of a coating to the material’s surface. The effectiveness and durability of such coatings need to be tested. When defects form on the coating’s surface, these become the corrosion hot spots of the inadequately protected metal. EIS is a very suitable detector of a coating’s condition because of its sensitivity to capacitance changes. Many coating EIS analyses focus on the parameter  $\alpha$  of a CPE as an indicator for the coating quality of some coating types. EIS measurements over a broad

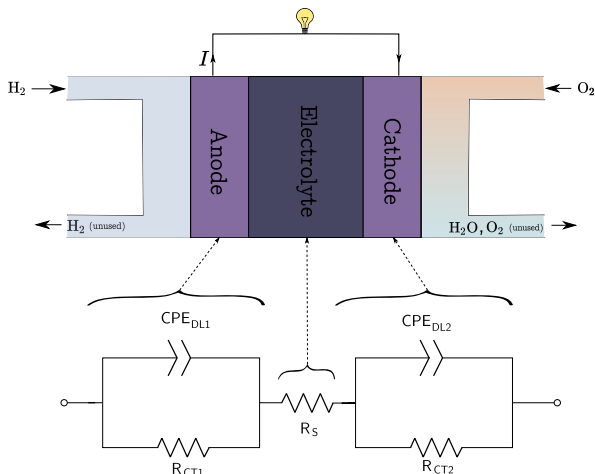


FIGURE 5. Basic fuel cell equivalent circuit. The two ZARC elements represent the electrochemical behaviour of the anode and cathode, whereas the resistor  $R_S$  models the resistance of the fuel cell’s electrolyte.

frequency range can identify the electrochemical characteristics of coating materials, metal substrates, surface films, and their polarizability. As such, information on a coating's condition, degradation, film development, and metal corrosion is acquired. A large body of research supports the use of EIS in corrosion monitoring [1], [102], [103]. An important parameter in EIS corrosion characterization is the polarisation resistance value  $R_p$ , which EIS can determine using an equivalent electrical circuit. The polarisation resistance of a freely corroding metal is inversely proportional to the corrosion rate. The presentation of the associated equivalent circuit is essential when reporting polarisation resistances in corrosion studies. An example of such a circuit is shown in Fig. 7. A representative general frequency range for corrosion studies is 100mHz to 100kHz.

## 2) CONSTRUCTION MATERIALS

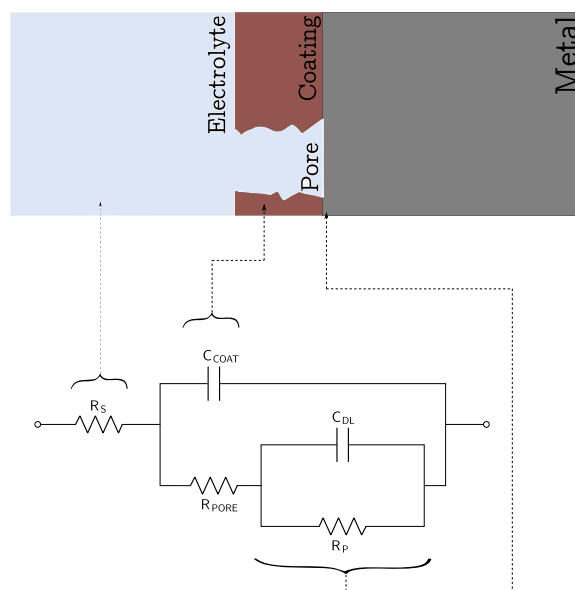
Micro-structural changes in cementitious materials (e.g., air voids, capillary pores, and gel pores) resulting from their chemical environment are reflected in their impedance spectra. Research on the application of EIS to analyze cement mortar and (reinforced) concrete started in the 1980s. It has been used to non-destructively investigate the cement hydration, porosity, ionic conductivity, pore structure, and durability (e.g., carbonation behaviour [104]) of concrete in addition to other parameters of interest, which relate to the performance of the construction materials [105]–[108]. The Debye circuit has been used in cement hardening studies [109]. In this circuit, a capacitor  $C_1$  relates to the sample geometry and a resistor  $R_2$  connected to another capacitor  $C_1$  is associated with the ionic motion of electrolyte in the pores. Cement porosity can be evaluated through its dielectric constant, which is proportional to  $C_1$ . For nondestructive cement hydration monitoring, the Randles circuit, Gu's equivalent circuit [110] and Zhang *et al.*'s modification thereof [111] have been reported. This modified version is displayed in Fig. 8. Frequencies in the order of up to several MHz are used in this application.

## D. BIOLOGICAL, MEDICAL AND FOOD APPLICATIONS

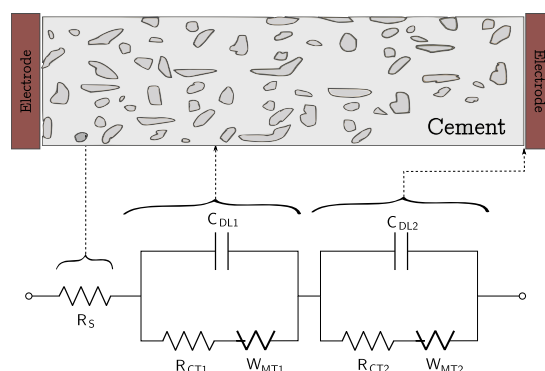
Grossi and Riccò [112] and Prasad and Roy [113] have reviewed some of the applications of bio-impedance spectroscopy. The present work focuses on the applied equivalent circuits and their domain-specific interpretations. A useful overview of commonly used equivalent circuits in bio-impedance applications from a fractional calculus perspective was conducted by T.J. Freeborn [61]. Based on the number of published works, the importance of EIS in the food industry is on the rise. Meat freshness and quality assessment are two key applications that benefit from this non-invasive and sensitive technique. Product evaluation and quality assessment in agriculture also increasingly feature EIS.

## 1) PLANTS

The characterization of various plant properties through EIS measurement dates back to the middle of the twentieth



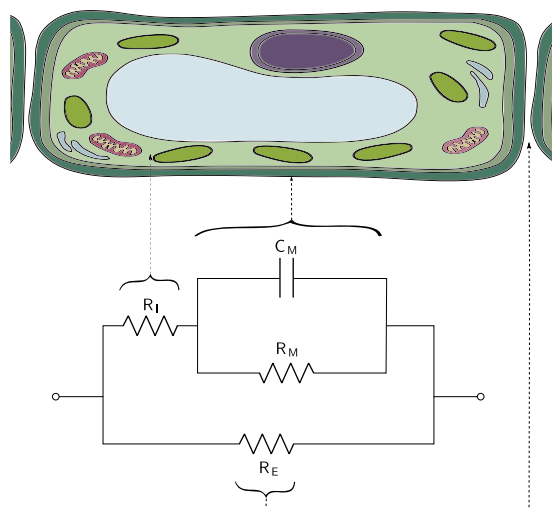
**FIGURE 7.** Generic coating equivalent circuit model, where the capacitors are often replaced by CPEs when modelling real systems in practice.  $R_S$  models the electrolyte resistance,  $C_{DL}$  and  $R_P$  are the double-layer capacitance and polarisation resistance that model corrosion at the metal surface,  $C_{COAT}$  is the coating capacitance, and  $R_{PORE}$  models the resistance that hinders the electrolyte from reaching the metal surface through the pores in the coating.



**FIGURE 8.** The modified version of Gu's equivalent circuit for cement characterization. Here,  $R_S$  models the electrolyte solution resistance,  $C_{DL1}$  is the double-layer capacitance between the cement's solid and liquid phases,  $C_{DL2}$  is the double-layer capacitance at the cement-electrode interface, and  $R_{CT1}$ - $W_{MT1}$  and  $R_{CT2}$ - $W_{MT2}$  are the Faradaic impedances modelling charge transfer and diffusion in cement and at the cement-electrode interface, respectively. This circuit has been applied to fit impedance spectra over a frequency range of 0.01Hz to 1MHz.

century and has continued to gain traction ever since. The passive electrical properties of plant tissues cause their impedance measurements to be related to cellular ionic current, membrane structures, and viscosity. This allows for a wide range of plant characteristics and processes to be investigated using EIS. Within the frequency range of 10 Hz to 1 MHz, three main factors influence the impedance measurements of plant tissues:

- (i) Symplastic (intercellular) resistance.
- (ii) Apoplastic (extracellular) resistance.
- (iii) Cell membrane capacitive reactance.



**FIGURE 9.** Hayden equivalent circuit model of plant cells, consisting of the intercellular resistance  $R_I$ , the membrane resistance  $R_M$ , the membrane capacitance  $C_M$ , and the extracellular resistance  $R_E$ .

The Hayden model [114] displayed in Fig. 9 is a historical equivalent electrical circuit model that includes components corresponding to these three factors, with the addition of a membrane resistance. More recently developed equivalent electrical circuit models are the simplified Hayden models [115] and the double-shell model [116]. The simplified Hayden model considers the membrane resistance to be negligible and model the membrane impedance with a capacitor or CPE, whereas the double-shell model takes the impedance due to the vacuoles of the plant cells into account. Here a serially connected resistor and capacitor are connected in parallel with the intracellular resistance ( $R_I$ ). These additional circuit components correspond to the plant cell's vacuolar resistance and its tonoplast's capacitance. Applications of EIS in plant science [3] include, but are not limited to, root growth estimation, frost hardening capability evaluation, plant-based food quality assessment [117], fruit ripening [118], [119], and (a)biotic stress detection. Variations on the Hayden model are typically applied in studies aiming to characterize some plant properties. Unlike many other EIS application domains, the Randles circuit is rarely applied as an out-of-the-box circuit here. In some cases, very simple and interpretable circuits consisting of three components are applied, while in other cases, complex non-interpretable circuits that are capable of modelling the impedance behavior are used [117]. An example of a frequency range for a plant application is several hundred Hz to several MHz.

## 2) BIOSENSORS

Biosensors are devices that make use of biological molecules, such as proteins [120]–[122] and nucleic acids, to detect and quantify the presence of analytes. They are the most prominent biological application of EIS because they allow for the sensitive and selective detection of microorganisms and bio-molecules, without some of the inconveniences that such detection methods typically entail. EIS-based biosensors can be implemented for practical applications at relatively

low cost and do not require the extensive sample preparation procedures that constitute traditional bio-molecule detection methods such as those based on an enzyme-linked immunosorbent assay (ELISA) or reverse transcriptase polymerase chain reaction (RT-PCR). Affinity-binding events are directly detected through interfacial changes at the electrode surface. The use of biosensors also does not require well-trained technicians and laboratory facilities, as opposed to its aforementioned alternatives. To date, EIS-based biosensors have been developed for the detection of undesirable food-borne pathogens [123], [124], such as noroviruses [125], *Salmonella* Typhimurium [126], [127], *Listeria monocytogenes* [128], and *E. coli* O157 [129], [130]. Biosensors are also being applied for the detection of other microorganisms of medical concern, some notable ones being *Staphylococcus aureus* [129], [131], [132], avian influenza [133] and the Dengue virus [134]. Besides the sensitive and label-free (i.e., not requiring gold nanoparticles or fluorescent tags) detection of undesirable bacteria and viruses, EIS-based biosensors are also being put into use as *genosensors* capable of detecting DNA hybridization, as well as protein sensors.

While the literature about impedimetric biosensors is extensive, the focus in such works is usually on the development of the hardware of such systems. There is a notable uniformity in the equivalent electrical circuits used by researchers in this application domain. Some standard circuits are used with limited variation. The general standard EEC which incurs limited variation throughout the literature is the modified Randles circuit shown in Fig. 1a. In applications concerning bacterial biosensors, often only the charge-transfer resistance parameter  $R_{CT}$  is used for further analysis. [135], [136]. In some of these cases the EEC from which the charge transfer resistance originates is not mentioned, presumably due to the ubiquitous usage of the Randles circuit [137]. A representative frequency range for this application is 0.1Hz to 100kHz, with occasional variations of one order of magnitude.

## 3) ANIMALS AND MEDICINE

The impact of bioelectrochemistry on medicine has become substantial and continues to increase. EIS analysis has been shown to be an effective tool in medical applications such as the investigation of human neural cells [138], characterization of the state of organs (e.g., liver) [139], and impedance analysis of skin [140]–[142] and muscular tissue [143]. Due to its use of small excitation signal amplitudes, EIS can safely provide a lot of information in a non-invasive manner. Its safety is a clear advantage over alternative non-invasive modalities that emit harmful radiation. The difficulties in the medical sector include the limitation of the current below the perception threshold, maintaining the non-invasive aspect of EIS. Furthermore, humans and animals continuously change their state (i.e., through movement, circulation, respiration, etc.), requiring fast measurement are typically being applied in animal and biomedical settings [144]–[147].

The Fractional single and double dispersion Cole circuits described in Section III often feature in these applications. The lower limit of the frequency in animal applications is usually several hundred to several thousand kHz.

#### IV. ACCOMPANYING SOFTWARE

The software developed for this work is an extension of the previously developed `EquivalentCircuits.jl` package, called `circuit_search` and consists of comparing impedance measurements to the simulated impedance spectra of a library of fitted circuits, covering all the application domains considered in this work. It allows users to automatically search for domain-specific equivalent circuits that fit their EIS measurement data while simultaneously providing them with the relevant literature from which the circuits originate. In this way, practitioners can evaluate whether the physical interpretation of the found circuits conforms with the investigated electrochemical system. The parameters of the circuits are identified using the two-step optimization procedure described in Section I-C, in combination with the objective function described by Eq. (10). We implemented the software using Julia, which is a relatively new and computationally efficient programming language [148]. More information and documentation of the software can be found at <https://github.com/MaximeVH/EquivalentCircuits.jl>.

#### V. DISCUSSION

Upon inspection of the various EECs, some commonalities in circuit topology can be distinguished. All interpretable and physically motivated equivalent circuit models seem to reside within a limited region in the space of possible circuit topologies. The circuits frequently feature a variant of the fractional ZARC element and rarely contain parallel loops nested deeper than three levels. A trend in all research areas is the lack of agreement and consistency in equivalent circuits used to analyze similar electrochemical systems as well as the use of different units (and different impedance expressions) for component parameters, making the comparison between studies more difficult. One of the factors limiting the development of EIS measurement analysis methods (and the transfer of progress among research domains) is the minimal public availability of experimental EIS data. This prevents researchers from different EIS application domains from comparing and evaluating their methods with data from other research areas. Good practice in EIS data analysis dictates that the Kramers–Kronig relations should be satisfied in the frequency range of interest to warrant an interpretable measurement data analysis, with the optional additional use of some other modern data validation methods. If the data does not satisfy the KK relations, the system does not comply with an EIS experiment's linearity, stationarity, or causality requirements. An evaluation of the Kramers–Kronig relations should be reported in EIS studies.

EECs represent a practical compromise between physical (electrochemical) models, which require a considerable amount of system-specific physics background and research to understand and implement but are fully interpretable on

the one hand, and machine learning models that are good at modelling the data but are lacking in physical interpretation and understanding of electrochemical systems, while also requiring a larger amount of data to train on the other hand. Another challenge for machine learning models in EIS is that instrumentation and other settings are rarely reproduced well (i.e., there are large variations in the measurement setups). A machine learning model can fit the EIS response of a given EIS setting, but the applicability cannot necessarily be generalized to other experimental settings. Even small variations in the measurement setup are reflected in the impedance spectra [149]. The measured frequencies for animal and plant applications are comparatively higher. This is partly due to the system's stability requirement, which does not always hold for biological systems at low frequencies. Exact physical models, with partial differential equations explaining the cell's potential based on electrochemical reactions in the cell, are not readily available in most settings. EEC models also have a meager computational cost in comparison. In cases such as system monitoring applications where the exact mechanistic understanding of the underlying electrochemical processes is of lesser importance, it could be advisable, performance-wise, to apply alternative state-of-the-art data-driven models rather than designing overly complex and uninterpretable equivalent circuit models to forcefully fit the measurements, losing any physical meaning.

As all the applications of EIS deal with electrochemical systems in some shape or form, it should come as no surprise that there are many interfaces and links between the application areas, which could be exploited in further research. Since most advances in EIS data analysis have been made for power sources, efforts should be made to translate these developments to other domains of application. An example of such a development is the DRT method, for which research to mitigate its flaws is progressing rapidly. Publicly available implementations of this method are available online [37]. EIS is already inherently a multidisciplinary science with a broad application range over different fields and non-standardized conventions, e.g., circuit representation, and the standard replacement of capacitors with CPEs in most real systems. Differences in terminology hinder the efficient transfer of progress between domains. Note, however, that application domains will exploit different strengths of EIS. Furthermore, Some differences among application domains are purely due to the application itself and not due to a lack of standardization or progress transfer.

#### VI. CONCLUSION

Appropriate EECs allow practitioners to obtain results of sufficient quality without incurring an excessively large computational burden. We have critically compared and reviewed the use of equivalent electrical circuits in published research, spanning various scientific fields. We have conducted an insightful comparison of the used equivalent circuits along with their corresponding interpretation and simulated impedance spectra and encouraged the

communication and transfer of progress across the different application domains. Recent trends and developments in the data analysis of electrochemical impedance spectroscopy measurements featuring equivalent circuits have also been discussed.

## REFERENCES

- [1] Y. Hamlaoui, F. Pedraza, and L. Tifouti, "Corrosion monitoring of galvanised coatings through electrochemical impedance spectroscopy," *Corrosion Sci.*, vol. 50, no. 6, pp. 1558–1566, Jun. 2008.
- [2] R. Xiong, J. Cao, Q. Yu, H. He, and F. Sun, "Critical review on the battery state of charge estimation methods for electric vehicles," *IEEE Access*, vol. 6, pp. 1832–1843, 2017.
- [3] I. Jócsák, G. Végvári, and E. Vozáry, "Electrical impedance measurement on plants: A review with some insights to other fields," *Theor. Exp. Plant Physiol.*, vol. 31, no. 3, pp. 359–375, Sep. 2019.
- [4] V. F. Lvovich, *Impedance Spectroscopy: Applications to Electrochemical and Dielectric Phenomena*. Hoboken, NJ, USA: Wiley, 2012.
- [5] M. E. Orazem and B. Tribollet, *Electrochemical Impedance Spectroscopy The Electrochemical Society Series*. Hoboken, NJ, USA: Wiley, 2008.
- [6] E. Barsoukov and J. R. Macdonald, *Impedance Spectroscopy: Theory, Experiment, and Applications*. Hoboken, NJ, USA: Wiley, 2018.
- [7] D. D. Macdonald, "Reflections on the history of electrochemical impedance spectroscopy," *Electrochim. Acta*, vol. 51, nos. 8–9, pp. 1376–1388, Jan. 2006.
- [8] F. Lisdat and D. Schäfer, "The use of electrochemical impedance spectroscopy for biosensing," *Anal. Bioanal. Chem.*, vol. 391, no. 5, pp. 1555–1567, Apr. 2008.
- [9] S. Wang, J. Zhang, O. Gharbi, V. Vivier, M. Gao, and M. E. Orazem, "Electrochemical impedance spectroscopy," *Nature Rev. Methods Primers*, vol. 1, 2021, Art. no. 41.
- [10] H. Helmholtz, "Ueber einige gesetze der vertheilung elektrischer ströme in körperlichen leitern mit anwendung auf die thierisch-elektrischen versuche," *Annalen der Physik und Chem.*, vol. 165, no. 6, pp. 211–233, 1853.
- [11] J. Sabatier, M. Merveillaut, J. M. Francisco, F. Guillemard, and D. Porcelatto, "Lithium-ion batteries modeling involving fractional differentiation," *J. Power Sources*, vol. 262, pp. 36–43, Sep. 2014.
- [12] J. Bisquert, "Influence of the boundaries in the impedance of porous film electrodes," *Phys. Chem. Chem. Phys.*, vol. 2, no. 18, pp. 4185–4192, 2000.
- [13] M. Crescentini, A. De Angelis, R. Ramilli, G. De Angelis, M. Tartagni, A. Moschitta, P. A. Traverso, and P. Carbone, "Online EIS and diagnostics on lithium-ion batteries by means of low-power integrated sensing and parametric modeling," *IEEE Trans. Instrum. Meas.*, vol. 70, 2021, Art. no. 2001711.
- [14] M. Messing, T. Shoa, and S. Habibi, "Estimating battery state of health using electrochemical impedance spectroscopy and the relaxation effect," *J. Energy Storage*, vol. 43, Nov. 2021, Art. no. 103210.
- [15] M. Van Haevebeke, M. Stock, and B. De Baets, "Practical equivalent electrical circuit identification for electrochemical impedance spectroscopy analysis with gene expression programming," *IEEE Trans. Instrum. Meas.*, vol. 70, 2021, Art. no. 2514612.
- [16] J. Olarte, J. M. de Ilarduya, E. Zulueta, R. Ferret, U. Fernández-Gámiz, and J. M. Lopez-Guede, "Automatic identification algorithm of equivalent electrochemical circuit based on electroscopic impedance data for a lead acid battery," *Electronics*, vol. 10, no. 11, p. 1353, Jun. 2021.
- [17] M. A. Danzer and E. P. Hofer, "Electrochemical parameter identification—An efficient method for fuel cell impedance characterisation," *J. Power Sources*, vol. 183, no. 1, pp. 55–61, Aug. 2008.
- [18] P. Büschel, T. Günther, and O. Kanoun, "Distribution of relaxation times for effect identification and modeling of impedance spectra," in *Proc. IEEE Int. Instrum. Meas. Technol. Conf. (I2MTC)*, May 2014, pp. 901–904.
- [19] M. Žic, "Solving CNLS problems by using Levenberg–Marquardt algorithm: A new approach to avoid off-limits values during a fit," *J. Electroanal. Chem.*, vol. 799, pp. 242–248, Aug. 2017.
- [20] F. González, D. Greiner, V. Mena, R. M. Souto, J. J. Santana, and J. J. Aznárez, "Fitting procedure based on differential evolution to evaluate impedance parameters of metal-coating systems," *Eng. Comput.*, vol. 36, no. 9, pp. 2960–2982, Nov. 2019.
- [21] F. M. Janeiro and P. M. Ramos, "A comparative analysis between genetic algorithms and complex nonlinear least squares on electrical impedance characterization," in *Proc. IEEE Int. Instrum. Meas. Technol. Conf.*, May 2016, pp. 1–6.
- [22] M. Kowski and M. J. Palys, "Genetic algorithm-based improvement to equivalent circuit analysis of experimental data in electrochemical impedance spectroscopy," *ChemElectroChem*, vol. 8, no. 15, pp. 2956–2967, Aug. 2021.
- [23] J. Yu, H. Cao, and Y. He, "A new tree structure code for equivalent circuit and evolutionary estimation of parameters," *Chemometric Intell. Lab. Syst.*, vol. 85, no. 1, pp. 27–39, Jan. 2007.
- [24] M. Keddad, H. Takenouti, X. R. Nóvoa, C. Andrade, and C. Alonso, "Impedance measurements on cement paste," *Cement Concrete Res.*, vol. 27, no. 8, pp. 1191–1201, Aug. 1997.
- [25] M. Žic and S. Pereverzyev, "Optimizing noisy CNLS problems by using nelder-mead algorithm: A new method to compute simplex step efficiency," *J. Electroanal. Chem.*, vol. 851, Oct. 2019, Art. no. 113439.
- [26] A. Nasser-Eddine, B. Huard, J.-D. Gabano, and T. Poinot, "A two steps method for electrochemical impedance modeling using fractional order system in time and frequency domains," *Control Eng. Pract.*, vol. 86, pp. 96–104, May 2019.
- [27] C. F. Zou, L. Zhang, X. Hu, Z. Wang, T. Wik, and M. Pecht, "A review of fractional-order techniques applied to lithium-ion batteries, lead-acid batteries, and supercapacitors," *J. Power Sources*, vol. 390, pp. 286–296, Jun. 2018.
- [28] P. Büschel, U. Tröltzsch, and O. Kanoun, "Use of stochastic methods for robust parameter extraction from impedance spectra," *Electrochim. Acta*, vol. 56, no. 23, pp. 8069–8077, Sep. 2011.
- [29] B. Wang, S. E. Li, H. Peng, and Z. Liu, "Fractional-order modeling and parameter identification for lithium-ion batteries," *J. Power Sources*, vol. 293, pp. 151–161, Oct. 2015.
- [30] J. Roth, M. Slocinski, and J. Luy, "Modeling Li-ion battery aging data utilizing particle swarm optimization," *Lect. Notes Impedance Spectrosc. II*, vol. 2, pp. 1–11, Jun. 2010.
- [31] M. Slocinski, K. Kögel, and J.-F. Luy, "Distance measure for impedance spectra for quantified evaluations," *Lect. Notes Impedance Spectrosc. III*, vol. 3, pp. 1–11, Jun. 2012.
- [32] F. M. Janeiro, J. Santos, and P. M. Ramos, "Gene expression programming in sensor characterization: Numerical results and experimental validation," *IEEE Trans. Instrum. Meas.*, vol. 62, no. 5, pp. 1373–1381, May 2013.
- [33] S. F. Lempka, S. Miocinovic, M. D. Johnson, J. L. Vitek, and C. C. McIntyre, "In vivo impedance spectroscopy of deep brain stimulation electrodes," *J. Neural Eng.*, vol. 6, no. 4, Aug. 2009, Art. no. 046001.
- [34] M. Kunaver, M. Žic, I. Fajfar, T. Tuma, Á. Búrmen, V. Subotić, and Ž. Rojec, "Synthesizing electrically equivalent circuits for use in electrochemical impedance spectroscopy through grammatical evolution," *Processes*, vol. 9, no. 11, p. 1859, Oct. 2021.
- [35] B. Agudelo, W. Zamboni, E. Monmasson, and G. Spagnuolo, "Identification of battery circuit model from EIS data," in *Proc. JCGE-Congrès des Jeunes Chercheurs en Génie Electrique*, 2019, pp. 1–7.
- [36] M. Žic, S. Pereverzyev, V. Subotić, and S. Pereverzyev, "Adaptive multi-parameter regularization approach to construct the distribution function of relaxation times," *Int. J. Geomath.*, vol. 11, no. 1, pp. 1–23, Dec. 2020.
- [37] T. H. Wan, M. Saccoccio, C. Chen, and F. Ciucci, "Influence of the discretization methods on the distribution of relaxation times deconvolution: Implementing radial basis functions with DRTtools," *Electrochim. Acta*, vol. 184, pp. 483–499, Dec. 2015.
- [38] E. Ivers-Tiffée and A. Weber, "Evaluation of electrochemical impedance spectra by the distribution of relaxation times," *J. Ceram. Soc. Jpn.*, vol. 125, no. 4, pp. 193–201, 2017.
- [39] A. Leonide, V. Sonn, A. Weber, and E. Ivers-Tiffée, "Evaluation and modeling of the cell resistance in anode-supported solid oxide fuel cells," *J. Electrochem. Soc.*, vol. 155, no. 1, p. B36, 2008.
- [40] L. Wildfeuer, P. Gieler, and A. Karger, "Combining the distribution of relaxation times from EIS and time-domain data for parameterizing equivalent circuit models of lithium-ion batteries," *Batteries*, vol. 7, no. 3, p. 52, Aug. 2021.
- [41] Y. Zhang, Y. Chen, M. Li, M. Yan, M. Ni, and C. Xia, "A high-precision approach to reconstruct distribution of relaxation times from electrochemical impedance spectroscopy," *J. Power Sources*, vol. 308, pp. 1–6, Mar. 2016.

- [42] J. Liu and F. Ciucci, "The Gaussian process distribution of relaxation times: A machine learning tool for the analysis and prediction of electrochemical impedance spectroscopy data," *Electrochim. Acta*, vol. 331, Jan. 2020, Art. no. 135316.
- [43] J. Huang, M. Papac, and R. O'Hayre, "Towards robust autonomous impedance spectroscopy analysis: A calibrated hierarchical Bayesian approach for electrochemical impedance spectroscopy (EIS) inversion," *Electrochim. Acta*, vol. 367, Jan. 2021, Art. no. 137493.
- [44] E. Quattrocchi, T. H. Wan, A. Curcio, S. Pepe, M. B. Effat, and F. Ciucci, "A general model for the impedance of batteries and supercapacitors: The non-linear distribution of diffusion times," *Electrochim. Acta*, vol. 324, Nov. 2019, Art. no. 134853.
- [45] H. Zappen, F. Ringbeck, and D. Sauer, "Application of time-resolved multi-sine impedance spectroscopy for lithium-ion battery characterization," *Batteries*, vol. 4, no. 4, p. 64, Dec. 2018.
- [46] R. D. L. Kronig, "On the theory of dispersion of X-rays," *J. Opt. Soc. Amer.*, vol. 12, no. 6, pp. 547–557, 1927.
- [47] B. A. Boukamp, "A linear Kronig–Kramers transform test for imittance data validation," *J. Electrochem. Soc.*, vol. 142, no. 6, p. 1885, 1995.
- [48] M. Schönleber, D. Klotz, and E. Ivers-Tiffée, "A method for improving the robustness of linear Kramers–Kronig validity tests," *Electrochim. Acta*, vol. 131, pp. 20–27, Jun. 2014.
- [49] J. J. Giner-Sanz, E. M. Ortega, and V. Pérez-Herranz, "Total harmonic distortion based method for linearity assessment in electrochemical systems in the context of EIS," *Electrochim. Acta*, vol. 186, pp. 598–612, Dec. 2015.
- [50] M. E. Orazem, "A systematic approach toward error structure identification for impedance spectroscopy," *J. Electroanal. Chem.*, vol. 572, no. 2, pp. 317–327, Nov. 2004.
- [51] P. Jaccard, "The distribution of the flora in the Alpine zone," *New Phytol.*, vol. 11, no. 2, pp. 37–50, Feb. 1912.
- [52] A. Syropoulos, "Mathematics of multisets," in *Proc. Workshop Membrane Comput.* Berlin, Germany: Springer, 2000, pp. 347–358.
- [53] M. Senoussaoui, P. Kenny, T. Stafylakis, and P. Dumouchel, "A study of the cosine distance-based mean shift for telephone speech diarization," *IEEE/ACM Trans. Audio, Speech, Language Process.*, vol. 22, no. 1, pp. 217–227, Jan. 2014.
- [54] J. E. Schollée, E. L. Schymanski, M. A. Stravs, R. Gulde, N. S. Thomaidis, and J. Hollender, "Similarity of high-resolution tandem mass spectrometry spectra of structurally related micropollutants and transformation products," *J. Amer. Soc. Mass Spectrometry*, vol. 28, no. 12, pp. 2692–2704, Dec. 2017.
- [55] M. Mecozzi, M. Pietroletti, and Y. B. Monakhova, "FTIR spectroscopy supported by statistical techniques for the structural characterization of plastic debris in the marine environment: Application to monitoring studies," *Mar. Pollut. Bull.*, vol. 106, nos. 1–2, pp. 155–161, May 2016.
- [56] Y. Nagai, W. Y. Sohn, and K. Katayama, "An initial estimation method using cosine similarity for multivariate curve resolution: Application to NMR spectra of chemical mixtures," *Analyst*, vol. 144, no. 20, pp. 5986–5995, 2019.
- [57] M. E. Orazem, P. Agarwal, and L. H. Garcia-Rubio, "Critical issues associated with interpretation of impedance spectra," *J. Electroanal. Chem.*, vol. 378, nos. 1–2, pp. 51–62, Nov. 1994.
- [58] S. Fletcher, "Tables of degenerate electrical networks for use in the equivalent-circuit analysis of electrochemical systems," *J. Electrochem. Soc.*, vol. 141, no. 7, p. 1823, 1994.
- [59] S. Dierickx, A. Weber, and E. Ivers-Tiffée, "How the distribution of relaxation times enhances complex equivalent circuit models for fuel cells," *Electrochim. Acta*, vol. 355, Sep. 2020, Art. no. 136764.
- [60] Z. He and F. Mansfeld, "Exploring the use of electrochemical impedance spectroscopy (EIS) in microbial fuel cell studies," *Energy Environ. Sci.*, vol. 2, no. 2, pp. 215–219, 2009.
- [61] T. J. Freeborn, "A survey of fractional-order circuit models for biology and biomedicine," *IEEE J. Emerg. Sel. Topics Circuits Syst.*, vol. 3, no. 3, pp. 416–424, Sep. 2013.
- [62] I. Borg and P. J. Groenen, *Modern Multidimensional Scaling: Theory and Applications*. Berlin, Germany: Springer, 2005.
- [63] C. Rerolle and R. Wiart, "Kinetics of Pb and Pb-Ag anodes for zinc electrowinning—I. Formation of PbSO<sub>4</sub> layers at low polarization," *Electrochim. Acta*, vol. 40, no. 8, pp. 939–948, Jun. 1995.
- [64] M. Bojinov and B. Monahov, "Impedance measurements of the lead/sodium sulphate system: Synthesis of A.C. analogue circuit," *J. Power Sources*, vol. 30, nos. 1–4, pp. 287–299, 1990.
- [65] S. Cheng, J. Zhang, M. Zhao, and C. Cao, "Electrochemical impedance spectroscopy study of Ni/MH batteries," *J. Alloys Compounds*, vols. 293–295, pp. 814–820, Dec. 1999.
- [66] N. Meddings, M. Heinrich, F. Overney, J.-S. Lee, V. Ruiz, E. Napolitano, S. Seitz, G. Hinds, R. Raccichini, M. Gaberšček, and J. Park, "Application of electrochemical impedance spectroscopy to commercial Li-ion cells: A review," *J. Power Sources*, vol. 480, Dec. 2020, Art. no. 228742.
- [67] D. Andre, M. Meiler, K. Steiner, C. Wimmer, T. Soczka-Guth, and D. Sauer, "Characterization of high-power lithium-ion batteries by electrochemical impedance spectroscopy. I. Experimental investigation," *J. Power Sources*, vol. 196, no. 12, pp. 5334–5341, 2011.
- [68] L. Ungurean, G. Cârstoiu, M. V. Micea, and V. Groza, "Battery state of health estimation: A structured review of models, methods and commercial devices," *Int. J. Energy Res.*, vol. 41, no. 2, pp. 151–181, 2017.
- [69] R. Xiong, Y. Pan, W. Shen, H. Li, and F. Sun, "Lithium-ion battery aging mechanisms and diagnosis method for automotive applications: Recent advances and perspectives," *Renew. Sustain. Energy Rev.*, vol. 131, Oct. 2020, Art. no. 110048.
- [70] E. Din, C. Schaefer, K. Moffat, and J. Stauth, "A scalable active battery management system with embedded real-time electrochemical impedance spectroscopy," *IEEE Trans. Power Electron.*, vol. 32, no. 7, pp. 5688–5698, Jul. 2017.
- [71] B. Stiaszny, J. C. Ziegler, E. E. Krauß, J. P. Schmidt, and E. Ivers-Tiffée, "Electrochemical characterization and post-mortem analysis of aged LiMn<sub>2</sub>O<sub>4</sub>-Li(Ni<sub>0.5</sub>Mn<sub>0.3</sub>Co<sub>0.2</sub>)O<sub>2</sub>/graphite lithium ion batteries. Part I: Cycle aging," *J. Power Sources*, vol. 251, pp. 439–450, Apr. 2014.
- [72] D.-K. Kang and H.-C. Shin, "Investigation on cell impedance for high-power lithium-ion batteries," *J. Solid State Electrochem.*, vol. 11, no. 10, pp. 1405–1410, Oct. 2007.
- [73] O. A. Bangal, V. Chaturvedi, P. K. A. Babu, and M. V. Shelke, "Impedance analysis and equivalent circuit modelling of cells subjected to sinusoidal vibration test using electrochemical impedance spectroscopy," in *Proc. IEEE Transp. Electrific. Conf. (ITEC-India)*, Dec. 2019, pp. 1–6.
- [74] B. Fan, Z. Guan, H. Wang, L. Wu, W. Li, S. Zhang, and B. Xue, "Electrochemical processes in all-solid-state Li-S batteries studied by electrochemical impedance spectroscopy," *Solid State Ionics*, vol. 368, Oct. 2021, Art. no. 115680.
- [75] U. Morali and E. Salim, "Analysis of electrochemical impedance spectroscopy response for commercial lithium-ion batteries: Modeling of equivalent circuit elements," *Turkish J. Chem.*, vol. 44, no. 3, pp. 602–613, 2020.
- [76] L. A. Middlemiss, A. J. R. Rennie, R. Sayers, and A. R. West, "Characterisation of batteries by electrochemical impedance spectroscopy," *Energy Rep.*, vol. 6, pp. 232–241, May 2020.
- [77] T. Osaka, D. Mukoyama, and H. Nara, "Review—Development of diagnostic process for commercially available batteries, especially lithium ion battery, by electrochemical impedance spectroscopy," *J. Electrochem. Soc.*, vol. 162, no. 14, pp. A2529–A2537, 2015.
- [78] J. Häcker, C. Danner, B. Sievert, I. Biswas, Z. Zhao-Karger, N. Wagner, and K. A. Friedrich, "Investigation of magnesium–sulfur batteries using electrochemical impedance spectroscopy," *Electrochim. Acta*, vol. 338, Apr. 2020, Art. no. 135787.
- [79] J. Wang, H. Wang, and Y. Fan, "Techno-economic challenges of fuel cell commercialization," *Engineering*, vol. 4, no. 3, pp. 352–360, Jun. 2018.
- [80] K. Darowicki and L. Gawel, "Impedance measurement and selection of electrochemical equivalent circuit of a working PEM fuel cell cathode," *Electrocatalysis*, vol. 8, no. 3, pp. 235–244, May 2017.
- [81] W. Choi, P. N. Enjeti, and J. W. Howze, "Development of an equivalent circuit model of a fuel cell to evaluate the effects of inverter ripple current," in *Proc. 19th Annu. IEEE Appl. Power Electron. Conf. Expo. (APEC)*, vol. 1, Feb. 2004, pp. 355–361.
- [82] J. R. Selman and Y. P. Lin, "Application of AC impedance in fuel cell research and development," *Electrochim. Acta*, vol. 38, no. 14, pp. 2063–2073, Oct. 1993.
- [83] T. J. Freeborn, B. Maundy, and A. S. Elwakil, "Fractional-order models of supercapacitors, batteries and fuel cells: A survey," *Mater. Renew. Sustain. Energy*, vol. 4, no. 3, pp. 1–7, Sep. 2015.
- [84] Q. Wang, Z. Hu, L. Xu, J. Li, Q. Gan, X. Du, and M. Ouyang, "A comparative study of equivalent circuit model and distribution of relaxation times for fuel cell impedance diagnosis," *Int. J. Energy Res.*, vol. 45, no. 11, pp. 15948–15961, Sep. 2021.

- [85] L. Shi and M. L. Crow, "Comparison of ultracapacitor electric circuit models," in *Proc. IEEE Power Energy Soc. Gen. Meeting Convers. Del. Electr. Energy 21st Century*, Jul. 2008, pp. 1–6.
- [86] R. Martín, J. J. Quintana, A. Ramos, and I. de la Nuez, "Modeling of electrochemical double layer capacitors by means of fractional impedance," *J. Comput. Nonlinear Dyn.*, vol. 3, no. 2, Jan. 2008, Art. no. 021303.
- [87] H. Heydari, M. Abdouss, S. Mazinani, A. M. Bazargan, and F. Fatemi, "Electrochemical study of ternary polyaniline/MoS<sub>2</sub>-MnO<sub>2</sub> for supercapacitor applications," *J. Energy Storage*, vol. 40, Aug. 2021, Art. no. 102738.
- [88] C. Justin Raj, R. Manikandan, P. Sivakumar, D. O. Opar, A. D. Savariraj, W.-J. Cho, H. Jung, and B. C. Kim, "Origin of capacitance decay for a flower-like  $\delta$ -MnO<sub>2</sub> aqueous supercapacitor electrode: The quantitative surface and electrochemical analysis," *J. Alloys Compounds*, vol. 892, Feb. 2022, Art. no. 162199.
- [89] T. Ramesh, R. Vedarajan, N. Rajalakshmi, and L. R. G. Reddy, "Dynamic electrochemical impedance spectroscopy as a rapid screening tool for supercapacitor electrode materials," *J. Mater. Sci., Mater. Electron.*, vol. 31, no. 2, pp. 1681–1690, Jan. 2020.
- [90] S. Sahoo, P. Pazhamalai, K. Krishnamoorthy, and S.-J. Kim, "Hydrothermally prepared  $\alpha$ -MnSe nanoparticles as a new pseudocapacitive electrode material for supercapacitor," *Electrochim. Acta*, vol. 268, pp. 403–410, Apr. 2018.
- [91] P. Navalpotro, M. Anderson, R. Marcilla, and J. Palma, "Insights into the energy storage mechanism of hybrid supercapacitors with redox electrolytes by electrochemical impedance spectroscopy," *Electrochim. Acta*, vol. 263, pp. 110–117, Feb. 2018.
- [92] H. Ahmad, W. Y. Wan, and D. Isa, "Modeling the ageing effect of cycling using a supercapacitor-module under high temperature with electrochemical impedance spectroscopy test," *IEEE Trans. Rel.*, vol. 68, no. 1, pp. 109–121, Mar. 2019.
- [93] O. Gorduk, S. Gorduk, M. Gencten, M. Sahin, and Y. Sahin, "One-step electrochemical preparation of ternary phthalocyanine/acid-activated multiwalled carbon nanotube/polypyrrole-based electrodes and their supercapacitor applications," *Int. J. Energy Res.*, vol. 44, no. 11, pp. 9093–9111, Sep. 2020.
- [94] C. Zhang, A. Xie, W. Zhang, J. Chang, C. Liu, L. Gu, X. Duo, F. Pan, and S. Luo, "CuMn<sub>2</sub>O<sub>4</sub> spinel anchored on graphene nanosheets as a novel electrode material for supercapacitor," *J. Energy Storage*, vol. 34, Feb. 2021, Art. no. 102181.
- [95] O. Gorduk, M. Gencten, S. Gorduk, M. Sahin, and Y. Sahin, "Electrochemical fabrication and supercapacitor performances of metallo phthalocyanine/functionalized-multiwalled carbon nanotube/polyaniline modified hybrid electrode materials," *J. Energy Storage*, vol. 33, Jan. 2021, Art. no. 102049.
- [96] M. Jayachandran, A. Rose, T. Maiyalagan, N. Poongodi, and T. Vijayakumar, "Effect of various aqueous electrolytes on the electrochemical performance of  $\alpha$ -MnO<sub>2</sub> nanorods as electrode materials for supercapacitor application," *Electrochim. Acta*, vol. 366, Jan. 2021, Art. no. 137412.
- [97] P.-J. Han, Y.-F. Zhang, F. Y. Chen, and X.-H. Bai, "Interpretation of electrochemical impedance spectroscopy (EIS) circuit model for soils," *J. Central South Univ.*, vol. 22, no. 11, pp. 4318–4328, Nov. 2015.
- [98] J. Bonastre, J. Molina, J. C. Galván, and F. Cases, "Characterization of polypyrrole/phosphotungstate membranes by electrochemical impedance spectroscopy," *Synth. Met.*, vol. 187, pp. 37–45, Jan. 2014.
- [99] W.-C. Chen, T.-C. Wen, and A. Gopalan, "Negative capacitance for polyaniline: An analysis via electrochemical impedance spectroscopy," *Synth. Met.*, vol. 128, no. 2, pp. 179–189, Apr. 2002.
- [100] D. L. Shaffer, K. E. Feldman, E. P. Chan, G. R. Stafford, and C. M. Stafford, "Characterizing salt permeability in polyamide desalination membranes using electrochemical impedance spectroscopy," *J. Membrane Sci.*, vol. 583, pp. 248–257, Aug. 2019.
- [101] J. Evertsson, F. Bertram, L. Rullik, G. Harlow, and E. Lundgren, "Anodization of Al(100), Al(111) and Al alloy 6063 studied *in situ* with X-ray reflectivity and electrochemical impedance spectroscopy," *J. Electroanal. Chem.*, vol. 799, pp. 556–562, Aug. 2017.
- [102] R. W. Bosch, F. Moons, J. H. Zheng, and W. F. Bogaerts, "Application of electrochemical impedance spectroscopy for monitoring stress corrosion cracking," *Corrosion*, vol. 57, no. 6, pp. 532–539, Jun. 2001.
- [103] D. V. Ribeiro and J. C. C. Abrantes, "Application of electrochemical impedance spectroscopy (EIS) to monitor the corrosion of reinforced concrete: A new approach," *Construct. Building Mater.*, vol. 111, pp. 98–104, May 2016.
- [104] B. Dong, Q. Qiu, J. Xiang, C. Huang, F. Xing, and N. Han, "Study on the carbonation behavior of cement mortar by electrochemical impedance spectroscopy," *Materials*, vol. 7, no. 1, pp. 218–231, Jan. 2014.
- [105] M. Cabeza, P. Merino, A. Miranda, X. R. Nóvoa, and I. Sanchez, "Impedance spectroscopy study of hardened Portland cement paste," *Cement Concrete Res.*, vol. 32, no. 6, pp. 881–891, Jun. 2002.
- [106] I. Sánchez, X. R. Nóvoa, G. de Vera, and M. A. Climent, "Microstructural modifications in Portland cement concrete due to forced ionic migration tests. Study by impedance spectroscopy," *Cement Concrete Res.*, vol. 38, no. 7, pp. 1015–1025, Jul. 2008.
- [107] D. A. Koleva, J. H. W. de Wit, K. van Breugel, L. P. Veleva, E. van Westing, O. Copuroglu, and A. L. A. Fraaij, "Correlation of microstructure, electrical properties and electrochemical phenomena in reinforced mortar. Breakdown to multi-phase interface structures. Part II: Pore network, electrical properties and electrochemical response," *Mater. Characterization*, vol. 59, no. 6, pp. 801–815, Jun. 2008.
- [108] B. Díaz, L. Freire, P. Merino, X. R. Nóvoa, and M. C. Pérez, "Impedance spectroscopy study of saturated mortar samples," *Electrochim. Acta*, vol. 53, no. 25, pp. 7549–7555, Oct. 2008.
- [109] C. Andrade, V. M. Blanco, A. Collazo, M. Keddam, X. R. Nóvoa, and H. Takenouti, "Cement paste hardening process studied by impedance spectroscopy," *Electrochim. Acta*, vol. 44, no. 24, pp. 4313–4318, Jul. 1999.
- [110] P. Gu, P. Xie, and J. J. Beaudoin, "Microstructural characterization of the transition zone in cement systems by means of A.C. impedance spectroscopy," *Cement Concrete Res.*, vol. 23, no. 3, pp. 581–591, May 1993.
- [111] J. Zhang, F. Zheng, Z. Liu, S. Hong, B. Dong, and F. Xing, "Nondestructive monitoring on hydration behavior of cement pastes via the electrochemical impedance spectroscopy method," *Measurement*, vol. 185, Nov. 2021, Art. no. 109884.
- [112] M. Grossi and B. Riccò, "Electrical impedance spectroscopy (EIS) for biological analysis and food characterization: A review," *J. Sensors Sensor Syst.*, vol. 6, pp. 303–325, Aug. 2017.
- [113] A. Prasad and M. Roy, "Bioimpedance analysis of vascular tissue and fluid flow in human and plant body: A review," *Biosyst. Eng.*, vol. 197, pp. 170–187, Sep. 2020.
- [114] R. I. Hayden, C. A. Moyses, F. W. Calder, D. P. Crawford, and D. S. Fensom, "Electrical impedance studies on potato and alfalfa tissue," *J. Exp. Botany*, vol. 20, no. 2, pp. 177–200, 1969.
- [115] L. Wu, Y. Ogawa, and A. Tagawa, "Electrical impedance spectroscopy analysis of eggplant pulp and effects of drying and freezing-thawing treatments on its impedance characteristics," *J. Food Eng.*, vol. 87, no. 2, pp. 274–280, 2008.
- [116] M. I. N. Zhang and J. H. M. Willison, "Electrical impedance analysis in plant tissues," *J. Exp. Botany*, vol. 42, no. 11, pp. 1465–1475, 1991.
- [117] M. Islam, K. A. Wahid, A. V. Dinh, and P. Bhowmik, "Model of dehydration and assessment of moisture content on onion using EIS," *J. Food Sci. Technol.*, vol. 56, no. 6, pp. 2814–2824, Jun. 2019.
- [118] A. Chowdhury, P. Singh, T. K. Bera, D. Ghoshal, and B. Chakraborty, "Electrical impedance spectroscopic study of Mandarin orange during ripening," *J. Food Meas. Characterization*, vol. 11, no. 4, pp. 1654–1664, Dec. 2017.
- [119] A. D. Bauchot, F. R. Harker, and W. M. Arnold, "The use of electrical impedance spectroscopy to assess the physiological condition of kiwifruit," *Postharvest Biol. Technol.*, vol. 18, no. 1, pp. 9–18, 2000.
- [120] A. Kaushik, A. Yndart, S. Kumar, R. D. Jayant, A. Vashist, A. N. Brown, C.-Z. Li, and M. Nair, "A sensitive electrochemical immunosensor for label-free detection of zika-virus protein," *Sci. Rep.*, vol. 8, no. 1, Dec. 2018, Art. no. 9700.
- [121] M. Braiek, K. Rokhani, A. Chrouda, B. Mrabet, A. Bakhrouf, A. Maaref, and N. Jaffrezic-Renault, "An electrochemical immunosensor for detection of *Staphylococcus aureus* bacteria based on immobilization of antibodies on self-assembled monolayers-functionalized gold electrode," *Biosensors*, vol. 2, no. 4, pp. 417–426, Oct. 2012.
- [122] Y. Wang, Z. Ye, and Y. Ying, "New trends in impedimetric biosensors for the detection of foodborne pathogenic bacteria," *Sensors*, vol. 12, no. 3, pp. 3449–3471, Mar. 2012.
- [123] L. Lu, G. Chee, K. Yamada, and S. Jun, "Electrochemical impedance spectroscopic technique with a functionalized microwire sensor for rapid detection of foodborne pathogens," *Biosensors Bioelectron.*, vol. 42, pp. 492–495, Apr. 2013.
- [124] S. Puttaswamy and S. Sengupta, "Rapid detection of bacterial proliferation in food samples using microchannel impedance measurements at multiple frequencies," *Sens. Instrum. Food Qual. Saf.*, vol. 4, nos. 3–4, pp. 108–118, Dec. 2010.



- [125] S. H. Baek, M. W. Kim, C. Y. Park, C.-S. Choi, S. K. Kailasa, J. P. Park, and T. J. Park, "Development of a rapid and sensitive electrochemical biosensor for detection of human norovirus via novel specific binding peptides," *Biosensors Bioelectron.*, vol. 123, pp. 223–229, Jan. 2019.
- [126] J. Dong, H. Zhao, M. Xu, Q. Ma, and S. Ai, "A label-free electrochemical impedance immunosensor based on AuNPs/PAMAM-MWCNT-chi nanocomposite modified glassy carbon electrode for detection of *Salmonella typhimurium* in milk," *Food Chem.*, vol. 141, no. 3, pp. 1980–1986, Dec. 2013.
- [127] X. Ma, Y. Jiang, F. Jia, Y. Yu, J. Chen, and Z. Wang, "An aptamer-based electrochemical biosensor for the detection of *Salmonella*," *J. Microbiol. Methods*, vol. 98, pp. 94–98, Mar. 2014.
- [128] R. Wang, C. Ruan, D. Kanayeva, K. Lassiter, and Y. Li, "TiO<sub>2</sub> nanowire bundle microelectrode based impedance immunosensor for rapid and sensitive detection of listeria monocytogenes," *Nano Lett.*, vol. 8, no. 9, pp. 2625–2631, Sep. 2008.
- [129] F. Tan, P. H. M. Leung, Z.-B. Liu, Y. Zhang, L. Xiao, W. Ye, X. Zhang, L. Yi, and M. Yang, "A PDMS microfluidic impedance immunosensor for *E. coli O157: H7* and *Staphylococcus aureus* detection via antibody-immobilized nanoporous membrane," *Sens. Actuators B, Chem.*, vol. 159, no. 1, pp. 328–335, Nov. 2011.
- [130] Y. Wang, J. Ping, Z. Ye, J. Wu, and Y. Ying, "Impedimetric immunosensor based on gold nanoparticles modified graphene paper for label-free detection of *Escherichia coli O157: H7*," *Biosensors Bioelectron.*, vol. 49, pp. 492–498, Nov. 2013.
- [131] K. Bekir, H. Barhouni, M. Braiek, A. Chrouda, N. Zine, N. Abid, A. Maaref, A. Bakhrouf, H. B. Ouada, N. Jaffrezic-Renault, and H. B. Mansour, "Electrochemical impedance immunosensor for rapid detection of stressed pathogenic *Staphylococcus aureus* bacteria," *Environ. Sci. Pollut. Res.*, vol. 22, no. 20, pp. 15796–15803, 2015.
- [132] F. Jia, N. Duan, S. Wu, X. Ma, Y. Xia, Z. Wang, and X. Wei, "Impedimetric aptasensor for *Staphylococcus aureus* based on nanocomposite prepared from reduced graphene oxide and gold nanoparticles," *Microchim. Acta*, vol. 181, no. 9, pp. 967–974, 2014.
- [133] J. Lin, R. Wang, P. Jiao, Y. Li, Y. Li, M. Liao, Y. Yu, and M. Wang, "An impedance immunosensor based on low-cost microelectrodes and specific monoclonal antibodies for rapid detection of avian influenza virus H5N1 in chicken swabs," *Biosensors Bioelectron.*, vol. 67, pp. 546–552, May 2015.
- [134] A. E. K. Peh and S. F. Y. Li, "Dengue virus detection using impedance measured across nanoporous aluminum membrane," *Biosensors Bioelectron.*, vol. 42, pp. 391–396, Apr. 2013.
- [135] M. Golabi, F. Kuralay, E. W. H. Jager, V. Beni, and A. P. F. Turner, "Electrochemical bacterial detection using poly(3-aminophenylboronic acid)-based imprinted polymer," *Biosensors Bioelectron.*, vol. 93, pp. 87–93, Jul. 2017.
- [136] C. M. Pandey, I. Tiwari, V. N. Singh, K. N. Sood, G. Sumana, and B. D. Malhotra, "Highly sensitive electrochemical immunosensor based on graphene-wrapped copper oxide-cysteine hierarchical structure for detection of pathogenic bacteria," *Sens. Actuators B, Chem.*, vol. 238, pp. 1060–1069, Jan. 2017.
- [137] H. Jafari, M. Amiri, E. Abdi, S. L. Navid, J. Bouckaert, R. Jijie, R. Boukherroub, and S. Szunerits, "Entrapment of uropathogenic *E. coli* cells into ultra-thin sol-gel matrices on gold thin films: A low cost alternative for impedimetric bacteria sensing," *Biosensors Bioelectron.*, vols. 124–125, pp. 161–166, Jan. 2019.
- [138] K. Krulikiewicz, "Electrochemical impedance spectroscopy as a versatile tool for the characterization of neural tissue: A mini review," *Electrochem. Commun.*, vol. 116, Jul. 2020, Art. no. 106742.
- [139] E. Gersing, "Impedance spectroscopy on living tissue for determination of the state of organs," *Bioelectrochem. Bioenergetics*, vol. 45, no. 2, pp. 145–149, May 1998.
- [140] F. Clemente, P. Arpaia, and C. Manna, "Characterization of human skin impedance after electrical treatment for transdermal drug delivery," *Measurement*, vol. 46, no. 9, pp. 3494–3501, Nov. 2013.
- [141] L. Kubisz, D. Hojan-Jeziarska, M. Szewczyk, A. Majewska, W. Kawalkiewicz, E. Pankowski, M. Janus, J. Cwajda-Białasik, P. Mościcka, and A. Jawień, "In vivo electrical impedance measurement in human skin assessment," *Pure Appl. Chem.*, vol. 91, no. 9, pp. 1481–1491, Sep. 2019.
- [142] F. Lu, C. Wang, R. Zhao, L. Du, Z. Fang, X. Guo, and Z. Zhao, "Review of stratum corneum impedance measurement in non-invasive penetration application," *Biosensors*, vol. 8, no. 2, p. 31, 2018.
- [143] F. Clemente, M. Romano, P. Bifulco, and M. Cesarelli, "EIS measurements for characterization of muscular tissue by means of equivalent electrical parameters," *Measurement*, vol. 58, pp. 476–482, Dec. 2014.
- [144] B. Rigaud, L. Hamzaoui, M. R. Frikha, N. Chauveau, and J.-P. Morucci, "In vitro tissue characterization and modelling using electrical impedance measurements in the 100 Hz–10 MHz frequency range," *Physiol. Meas.*, vol. 16, no. 3A, pp. A15–A28, Aug. 1995.
- [145] Y. Ulgen and M. Sezdi, "Hematocrit dependence of the Cole–Cole parameters of human blood," in *Proc. 2nd Int. Conf. Biomed. Eng. Days*, 1998, pp. 71–74.
- [146] C. Tang, F. You, G. Cheng, D. Gao, F. Fu, and X. Dong, "Modeling the frequency dependence of the electrical properties of the live human skull," *Physiol. Meas.*, vol. 30, no. 12, p. 1293, 2009.
- [147] D. A. McRae, M. A. Esrick, and S. C. Mueller, "Changes in the noninvasive, in vivo electrical impedance of three xenografts during the necrotic cell-response sequence," *Int. J. Radiat. Oncol. Biol. Phys.*, vol. 43, no. 4, pp. 849–857, Mar. 1999.
- [148] J. Bezanson, A. Edelman, S. Karpinski, and V. B. Shah, "Julia: A fresh approach to numerical computing," *SIAM Rev.*, vol. 59, no. 1, pp. 65–98, 2017.
- [149] V. Muenzel, A. F. Hollenkamp, A. I. Bhatt, J. de Hoog, M. Brazil, D. A. Thomas, and I. Mareels, "A comparative testing study of commercial 18650-format lithium-ion battery cells," *J. Electrochem. Soc.*, vol. 162, no. 8, pp. A1592–A1600, 2015.



**MAXIME VAN HAEVERBEKE** received the B.Sc. and M.Sc. degrees in bioscience engineering from Ghent University, Belgium, in 2017 and 2019, respectively, where he is currently pursuing the Ph.D. degree in mathematical modeling. His research interests include machine learning, data analysis for electrochemical impedance spectroscopy, and the applications thereof.



**MICHEL STOCK** received the M.Sc. degree in bioscience engineering cell- and gene-biotechnology (major in computational biology) and the Ph.D. degree in machine learning from Ghent University. He is currently affiliated with the KERMIT and Biobix research units as a Postdoctoral Researcher. His research interests include computational intelligence and operational research toward understanding and designing complex biosystems.



**BERNARD DE BAETS** received the M.Sc. degree in mathematics, the postgraduate degree in knowledge technology, and the Ph.D. degree in mathematics from Ghent University, Belgium, in 1988, 1991, and 1995, respectively. He is currently a Senior Full Professor with Ghent University, where he is leading the Knowledge-Based Systems (KERMIT) Research Unit as well as the Department of Data Analysis and Mathematical Modelling. He has acted as a Supervisor of 86 Ph.D. students and has published over 600 peer-reviewed journal articles. He has delivered over 300 (invited) conference lectures. He is currently a Co-Editor-in-Chief of *Fuzzy Sets and Systems* and a member of the editorial board of several other journals. He is a Government of Canada Award holder; has been nominated for the Ghent University Prometheus Award for Research; and is a fellow of the International Fuzzy Systems Association, a recipient of the EUSFLAT Scientific Excellence Award, an Honorary Professor of Budapest Tech, an Honorary Member of EUSFLAT, a Doctor Honoris Causa of the University of Turku, a Professor Invitado of the Universidad Central "Marta Abreu" de Las Villas in Cuba, and a Professor Extraordinarius at the University of South Africa.